

TROPOMI Global NO₂ for urban and polluted areas globally Trends from TROPOMI (2019 to 2024): Urban Changes and Emerging Hotspots

Daniel E. Huber¹, Gaige H. Kerr¹, M. Omar Nawaz², Sara Runkel³, Susan C. Anenberg¹, Daniel L. Goldberg¹

¹Department Environmental and Occupational Health, Milken Institute School of Public Health, George Washington University, Washington, DC, USA

²School of Earth and Environmental Science, Cardiff University, Cardiff, United Kingdom

³National Center for Atmospheric Research, Boulder, CO, USA

Correspondence to: Daniel E. Huber (daniel.huber@gwu.edu)

Abstract. We present a global assessment of space-based urban nitrogen dioxide (NO₂) observation trends from 2019 to 2024 using annual and monthly mean tropospheric vertical column densities (VCDs) from the Tropospheric Monitoring Instrument (TROPOMI). Across 11,500 cities defined by the Global Human Settlement Layer-Settlement Model (GHS-SMOD), we find population-weighted annual mean urban NO₂ VCDs ~~declined between~~ were lower in 2024 than 2019 in Asia and 2024 in Asian Oceania (-17%), European% and Europe (-13%), and North American (-4%) cities, with seasonal decomposition indicating that ~~most of the~~ annual changes are largely driven by wintertime concentration decreases. Urban VCDs in North America, South American (-2%) America and Africa lacked a significant trend for the period, though numerous individual cities exhibited lesser population-weighted changes on average, while African (+3%) cities experienced a gradual increase in NO₂. Over this time frame significant trends. Of larger cities, Tehran had the largest annual mean NO₂ VCDs VCD (>30 × 10¹⁵ molecules cm⁻²) and Seoul had experienced the largest reduction (-40%). We further identify changes in NO₂ near fossil fuel operations and note conflict-related changes in NO₂, highlighting the responsiveness of satellite NO₂ to certain societal disruptions. 9.4 ± 1.0% yr⁻¹; p < 0.001). We then calculate NO₂ VCD urban enhancements (VCD_{ENH}) by removing background concentrations from urban signatures and compare VCD_{ENH} to changes in nitrogen oxide (NO_x) emissions from the Emissions Database for Global Atmospheric Research (EDGARv8.1), to highlight two emissions inventories, highlighting regions with potential inventory discrepancies. We find VCD_{ENH} and EDGARv8.1 changes exceed changes in inventory NO_x change at a similar rate from year to year emissions in Europe and, North America and Asia and Oceania, with worse agreement in the Global South. We further identify changes in NO₂ near fossil fuel operations and note conflict-related changes in NO₂, highlighting the responsiveness of satellite NO₂ to certain societal disruptions. This work demonstrates the value in space-based remote sensing being an accountability agent for air pollution emissions on a global scale and to identify changes in NO₂ in otherwise unmonitored regions.

31 1 Introduction

32 Nitrogen dioxide (NO₂) is a harmful air pollutant that originates from both anthropogenic and natural emissions sources,
33 including fossil fuel combustion, biomass burning, lightning, and soils (Dix et al., 2020; Jin et al., 2021; Schuman & Huntrieser,
34 2007; Huber et al., 2024), with fossil fuel combustion accounting for ~45% of total global nitrogen oxide emissions (Song et
35 al., 2021). Only a small amount of NO₂ is emitted from these sources directly, with nitric oxide (NO) being the primary
36 emissions product that quickly cycles to NO₂ in the presence of oxidants such as ozone (O₃) or peroxy radicals (HO₂ or RO₂).
37 The summed concentrations of NO and NO₂ are referred to as nitrogen oxides (NO_x = NO + NO₂), as the concentrations of
38 NO and NO₂ are inherently linked. NO₂ is more commonly targeted by regulatory measures than NO, as it constitutes the
39 majority of atmospheric NO_x concentrations and is linked to increased morbidity and mortality from long-term exposure,
40 particularly within urban environments (Chen et al., 2024). While NO_x is commonly associated with health risks, the direct
41 association between NO_x exposure and adverse health outcomes remains uncertain (Anenberg et al., 2022). Despite this, NO_x
42 contributes to known harmful secondary pollutants, including O₃ and fine particulate matter.

43 NO₂ concentrations are measured using: (1) in-situ monitoring, e.g. chemiluminescence analyzers at the surface, or (2) remote
44 sensing instrumentation leveraging the unique spectral properties of NO₂, that absorbs light most efficiently in the visible
45 portions (405 – 465 nm) of the electromagnetic spectrum (Lamsal et al., 2015). The latter method relies upon spectrometers
46 detecting in the UV-Visible spectral range to infer NO₂ vertical column densities (VCDs), defined as the summed concentration
47 of NO₂ in a column from the surface to an upper limit of the atmosphere, with the tropopause often used as the upper limit.
48 Spectrometers have been used to measure NO₂ VCDs from ground-level directed upward, from aircraft directed downward, or
49 from space-based satellites directed downward, including from the TROPOspheric Monitoring Instrument (TROPOMI)
50 onboard the Sentinel-5P satellite (Herman et al., 2009; Fishman et al., 2012; Veeffkind et al., 2012). NO₂ can also be remotely-
51 sensed from ground-based instruments capable of inferring vertical profiles of NO₂, such as using multi-axis differential optical
52 absorption spectroscopy (MAX-DOAS; Vlemmix et al., 2010).

53 The earliest space-based spectrometers detecting NO₂ were flown on low-earth polar orbiting satellites, and were launched
54 within the mid-1990s to mid-2000s. These include the Global Ozone Monitoring Experiment (GOME; Burrows et al., 1999)
55 and GOME-2 satellites, the SCanning Imaging Absorption spectroMeter for Atmospheric CHartographY (SCIAMACHY;
56 Bovensmann et al., 1999) and the Ozone Monitoring Instrument (OMI; Levelt et al., 2006). The data collected using these
57 instruments provided unique insight into atmospheric chemistry and composition across the globe, including in mostly
58 unmonitored regions. OMI, launched in 2004, provided NO₂ VCDs at a spatial resolution of 13 x 24 km² at nadir and has
59 remained operable for more than two decades at the time this was written, providing a valuable long-term record of NO₂
60 globally. OMI remained the highest resolution space-based NO₂ product until TROPOMI launched in 2017, which ultimately
61 provided NO₂ VCDs at a spatial resolution of 3.5 x 5.5 km² at nadir. Observations at this resolution facilitated the evaluation
62 of satellite NO₂ at previously unprecedented spatial scales, including at the intra-urban level (Goldberg et al., 2021; Goldberg
63 et al., 2024).

64 NO₂ trends have been characterized in urban and broader environments using space-based instruments. Earlier satellite studies
65 used the GOME and ~~SCIAMACHY~~ ~~SCIAMACHY~~ satellites to identify increasing NO₂ VCD trends in China from the mid-
66 1990s to the mid-2000s (Richter et al., 2005; Stavrakou et al., 2008; Van der A et al., 2008), driven primarily by economic
67 growth and industrialization. Later studies, incorporating OMI observations, highlighted further increases in China through the
68 early 2010s, with VCDs and satellite-inferred surface concentrations steadily declining since (Miyazaki et al., 2017; [Wang et
69 al., 2019](#); Jiang et al., 2022). Europe has exhibited steady NO₂ VCD declines since the start of the satellite NO₂ record (Richter
70 et al., 2005; Krotkov et al., 2016; Duncan et al., 2016), driven largely by the implementation of various emissions control
71 technologies. In the United States, NO₂ concentrations ~~increased through roughly~~ ~~generally exhibited a decreasing trend from~~
72 ~~2005, then decreased substantially~~ through the ~~early to~~ mid-2010s (Lamsal et al., 2015), with VCD decreases more gradual
73 since, in part due to an increased influence from regional background NO₂ levels (Jiang et al., 2018; [Dang et al., 2023](#)). [Goldberg
74 et al., 2021](#); [Dang et al., 2023](#)). [In contrast, urban regions of India have shown NO₂ increases over the past few decades, linked
75 to urbanization and energy demand growth \(Hilboll et al., 2013; Ghude et al., 2020\). Over Africa and South America, NO₂
76 VCD trends through the mid-2010s have been less pronounced, reflecting limited industrialization and more dominant
77 contributions from biomass burning and natural sources \(Geddes et al., 2016; Castellanos et al., 2014\).](#) Additionally, numerous
78 studies have highlighted the influence that the COVID-19 pandemic had on NO₂ globally, with most regions [globally](#) exhibiting
79 broad NO₂ decreases in 2020 during numerous lockdowns and subsequent, regionally-distinct rebounds in emissions (Lonsdale
80 et al., 2023; Fisher et al., 2024).

81 Satellite studies have been used to characterize trends within the urban environment specifically, using different methods to
82 characterize the urban extent. Geddes et al. (2016) used GOME, SCIAMACHY and GOME-2 oversampled to a 0.1° x 0.1°
83 grid to highlight NO₂ VCD trends globally, as well as in select urban areas, with the urban region defined as the surrounding
84 ~ 200 km x 200 km. Fioletov et al. (2022) and Fioletov et al. (2025) used urban density from the Gridded Population of the
85 World (SEDAC, 2017) as a proxy for the extent of the urban environment to identify changes in urban NO_x emissions.
86 Anenberg et al. (2022) used urban boundaries provided from the 2019 version of the Global Human Settlement Layer-
87 Settlement model (GHS-SMOD) to evaluate NO₂ trends from 2000 – 2019 using surface NO₂ estimates derived from
88 [TROPOMI](#) NO₂ and a land-use regression model.

89 Here, we use TROPOMI tropospheric NO₂ VCDs to quantify general NO₂ trends globally from 2019 to 2024, with a particular
90 focus on urban areas. The urban boundaries are defined by the 2023 version of GHS-SMOD, which provides urban cluster
91 boundaries for all urban regions globally. We evaluate urban NO₂ trends against ~~a~~-NO_x emissions [database, inventories](#) and
92 [evaluate characterize](#) the influence of different seasons on annual trends. We additionally note changes in select oil, gas, and
93 other mining regions, which exhibit the largest changes globally outside of urban areas. This study represents the first detailed
94 global-scale analysis of urban TROPOMI NO₂ trends from 2019 to 2024. Our findings illustrate how NO₂ responded to specific
95 societal events during this timeframe, such as the impact of clean air policies, population migration away from urban areas due
96 to war, the increased demand for fossil fuels and rare-Earth minerals, and the emergence and waning of a global pandemic.

97 Furthermore, by directly linking observed NO₂ urban enhancements with NO_x emission inventory data from the updated
98 EDGARv8.1, our work provides valuable insights into regions where emissions inventories align closely with observations, as
99 well as areas exhibiting potential inventory discrepancies. This work underscores the critical value of satellite-derived NO₂ as
100 a tool for urban air quality assessment and emissions management.

101 2 Data and Methods

102 2.1 Global Human Settlement Layer Urban Cluster Boundaries

103 The Global Human Settlement Layer-Settlement Model (GHS-SMOD; Schiavina et al., 2023) is a dataset developed by the
104 Joint Research Centre of the European Commission containing spatial boundaries and population estimates for all urban areas
105 globally with a population of at least 50,000, which can be used to subset gridded or spatially-disaggregated data for any built-
106 up area on Earth. GHS-SMOD uses satellite remote sensing to identify the spatial extent and boundaries of all cohesive built-
107 up areas globally at a spatial resolution of 1×1 km², with each separate, cohesive built-up area referred to as an “urban cluster”.
108 In this study, we use the terms “urban cluster” and “city” interchangeably, although we note that GHS-SMOD urban clusters
109 do not ~~necessarily align with administrative city boundaries.~~ always align with administrative city boundaries. GHS-SMOD
110 has the benefit of providing a globally consistent, satellite-derived definition of built-up areas, whereas administrative
111 boundaries vary widely in definition and availability. Using physical built-up area boundaries from GHS-SMOD instead of
112 administrative ones may shift the absolute spatial extent of some cities, but it does not materially alter the concentrations
113 calculated in this study.

114 The 2023 version of GHS-SMOD provides boundaries for approximately 11,500 urban clusters, along with population
115 estimates for the year 2020 (Fig. S1S8). We note that GHS-SMOD urban clusters do not reflect the traditional boundaries of
116 individual cities as we may understand them, and as such, GHS-SMOD urban clusters can span multiple cities, regions or even
117 countries. For example, the urban cluster encompassing San Diego, California includes the city of San Diego, but also the
118 adjacent surrounding suburbs, as well as the entirety of Tijuana, Mexico (Fig. S2S9). In such cases, attribution of an urban
119 cluster to one particular city is not possible.

120 We use the GHS-SMOD boundaries to subset monthly- and annually-averaged satellite NO₂ column concentration data for all
121 urban clusters, as described in Section 2.2.1.

122 2.2 TROPOMI NO₂ vertical column densities

123 The TROPOspheric Monitoring Instrument (TROPOMI) is a pushbroom spectrometer on board the Sentinel-5P satellite
124 traveling in low earth orbit, with approximately one overpass each afternoon (Veefkind et al., 2012). Launched in October,
125 2017, TROPOMI detects radiation in spectral bands ranging from the ultraviolet to shortwave infrared to infer concentrations
126 of various atmospheric constituents, including nitrogen dioxide (NO₂), which is best inferred from the near-UV and visible

127 portions of the spectrum. We use Level 3 monthly- and annually-averaged TROPOMI tropospheric NO₂ vertical column
128 densities (VCDs) on a 0.1° global grid (Goldberg, 2024), which were created by oversampling daily Level 2 TROPOMI NO₂
129 VCDs, ~~with a spatial resolution of 3.5 x 5.5 km² at nadir,~~ derived from version 2.4+ of the European Space Agency retrieval
130 algorithm (van Geffen et al., 2022). These Level 2 data have a nadir spatial resolution of 3.5 x 7.0 km² before and 3.5 x 5.5
131 km² after August 06, 2019. Data were quality controlled to remove Level 2 pixels with a qa_value < 0.75 before oversampling,
132 which removes data with quality issues related to clouds, surface reflectivity (e.g. snow and ice) or other retrieval errors. The
133 TROPOMI NO₂ data used in this study span six full calendar years from January 2019 to December 2024 (Fig. 1); we use the
134 RPRO version from 1 January 2019 – 25 July 2022 and the OFFL version from 26 July 2022 – 31 December 2024. On 7
135 September 2024 there was an update of the surface reflectivity assumptions and on 16 November 2024 there was an update to
136 the cloud retrieval, both of which induce a small positive step change in the data, but likely does not meaningfully affect the
137 2024 annual average.

138 TROPOMI NO₂ retrievals are subject to measurement and retrieval uncertainties that propagate into the oversampled Level 3
139 products. Typical uncertainties in monthly or annually averaged tropospheric NO₂ vertical column densities are on the order
140 of 15–20 %. Systematic biases have also been reported, with overestimation in less polluted regions (+26.5% bias) and
141 underestimation in areas with high NO₂ concentrations (-31.4% bias), reflecting limitations in the retrieval process (Glissenaar
142 et al., 2025; Lambert et al., 2025).

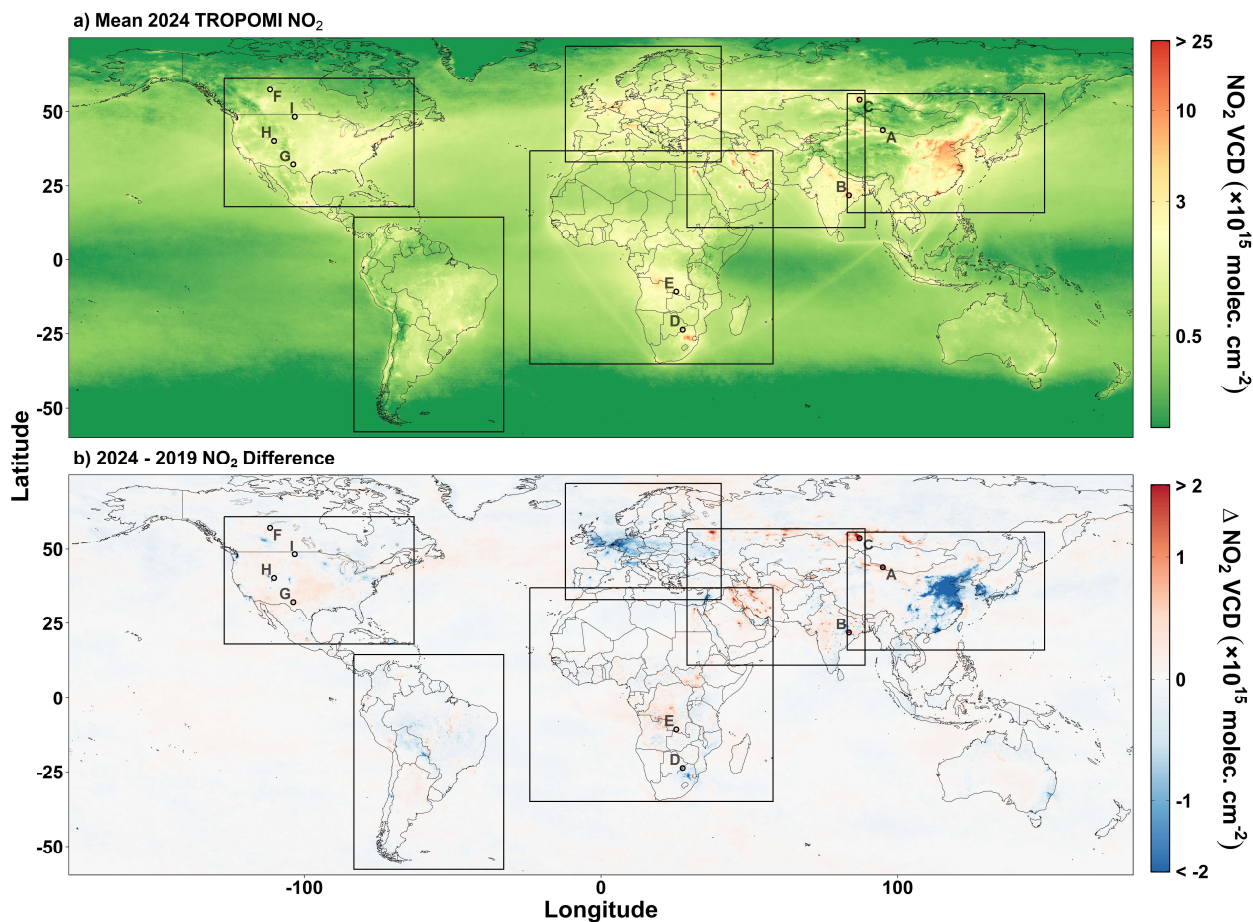


Figure 1: (a) Global 2024 annual average NO₂ VCDs colored on a log-scale and (b) the difference in VCD from 2019 to 2024 colored on a symmetric log-scale. Points labeled A-I correspond with locations of oil, gas and mining operations highlighted in Fig. 312. Boxes indicate select focus regions in Section 35.

2.2.13 Quantifying average TROPOMI NO₂ VCDs for GHS-SMOD urban clusters

For each urban cluster, we subset the oversampled TROPOMI data for grid cells that are located within 0.1° of the urban cluster boundary. For most cities, this results in approximately 20-25 grid cells, depending on the extent of the individual cluster. Given that the spatial resolution of GHS-SMOD is roughly an order of magnitude finer than that of the oversampled TROPOMI data (1 km vs. 0.1°) we interpolate the subsetting TROPOMI data to the 0.01° × 0.01° resolution of GHS-SMOD using a nearest neighbor approach. We then calculate an area-weighted average of interpolated grid cells that have a grid cell center falling within the urban cluster boundary (Fig. S2S9). This approach allows for the portions of oversampled 0.1° × 0.1° grid cells that may not be centered within an urban cluster boundary, but that still overlap with a cluster, to be accounted for within the average NO₂ column estimate.

156 To evaluate the changes in VCDs for broader regions, e.g. countries containing multiple urban clusters, we can calculate a
157 population-weighted average VCD, taking into account varying population sizes in different urban clusters.

$$158 \quad VCD_{PW} = \frac{\sum_i(POP_i \times VCD_i)}{\sum_i(POP_i)}, \quad (1)$$

159 In Eq. 1, VCD_{PW} represents the population-weighted VCD for a given country, POP_i represents the 2020 GHS-SMOD-
160 estimated population for a given urban cluster i , and VCD_i represents the mean NO_2 VCD for i .

161 For each time series, we use monthly TROPOMI NO_2 columns from 2019–2024 to estimate a linear trend in % yr^{-1} . We first
162 construct a de-seasonalized anomaly series by computing, for each calendar month at each location, the mean NO_2 over the
163 full period and expressing each monthly value as a percent deviation from its corresponding monthly mean. To obtain the
164 percent change per year and its standard error, we fit a linear regression to the original monthly series with time as the predictor
165 and fixed effects for calendar month to control for seasonality. The estimated annual percent change and its standard error were
166 taken directly from the time-slope coefficient and its standard error from this regression. To assess whether a statistically
167 significant trend was present, we regressed the de-seasonalized percent anomalies on time and obtained a p-value for the slope
168 using standard errors that account for temporal autocorrelation.

169 **2.34 Accounting for background NO_2**

170 To account for changes in upwind background NO_2 concentrations that may influence urban NO_2 VCDs, we quantify an urban
171 NO_2 enhancement.

$$172 \quad VCD_{ENH} = VCD_{UC} - VCD_{BG}, \quad (2)$$

173 In Eq. 2, VCD_{ENH} is the urban NO_2 VCD enhancement, VCD_{UC} is the NO_2 VCD within each urban cluster as described in
174 Section 2.2.1, and VCD_{BG} is the background concentration for an urban cluster. We define VCD_{BG} for a given year as the
175 10th–50th percentile of annual mean NO_2 VCDs extending 0.5 degrees in any direction from an Urban cluster boundary.
176 Previous studies have used a percentile threshold to determine background concentrations (de Gouw et al., 2020). See Section
177 S1 of the supplementary document for additional information and sensitivity tests regarding background VCD quantification.

178 **2.4 EDGAR5 NO_x emission emission inventories**

179 ~~We use~~ We use data from two inventories to evaluate NO_x emissions: (1) version 8.1 of the Emissions Database for Global
180 Atmospheric Research (EDGARv8.1; Crippa et al., 2024) to evaluate NO_x emissions, and (2) the 2025 version of Community
181 Emissions Data System (CEDS; Hoesly et al., 2025). EDGAR provides annual summed total and sector-specific NO_x
182 emissions at $0.1^\circ \times 0.1^\circ$ spatial resolution globally. ~~EDGAR NO_x emissions include contributions from, derived using a~~
183 bottom-up method that combines sector-level activity data with corresponding emissions factors for energy generation,
184 industrial sources, transportation, residential sources and agriculture. ~~EDGAR, with data available through 2022. CEDS is a~~

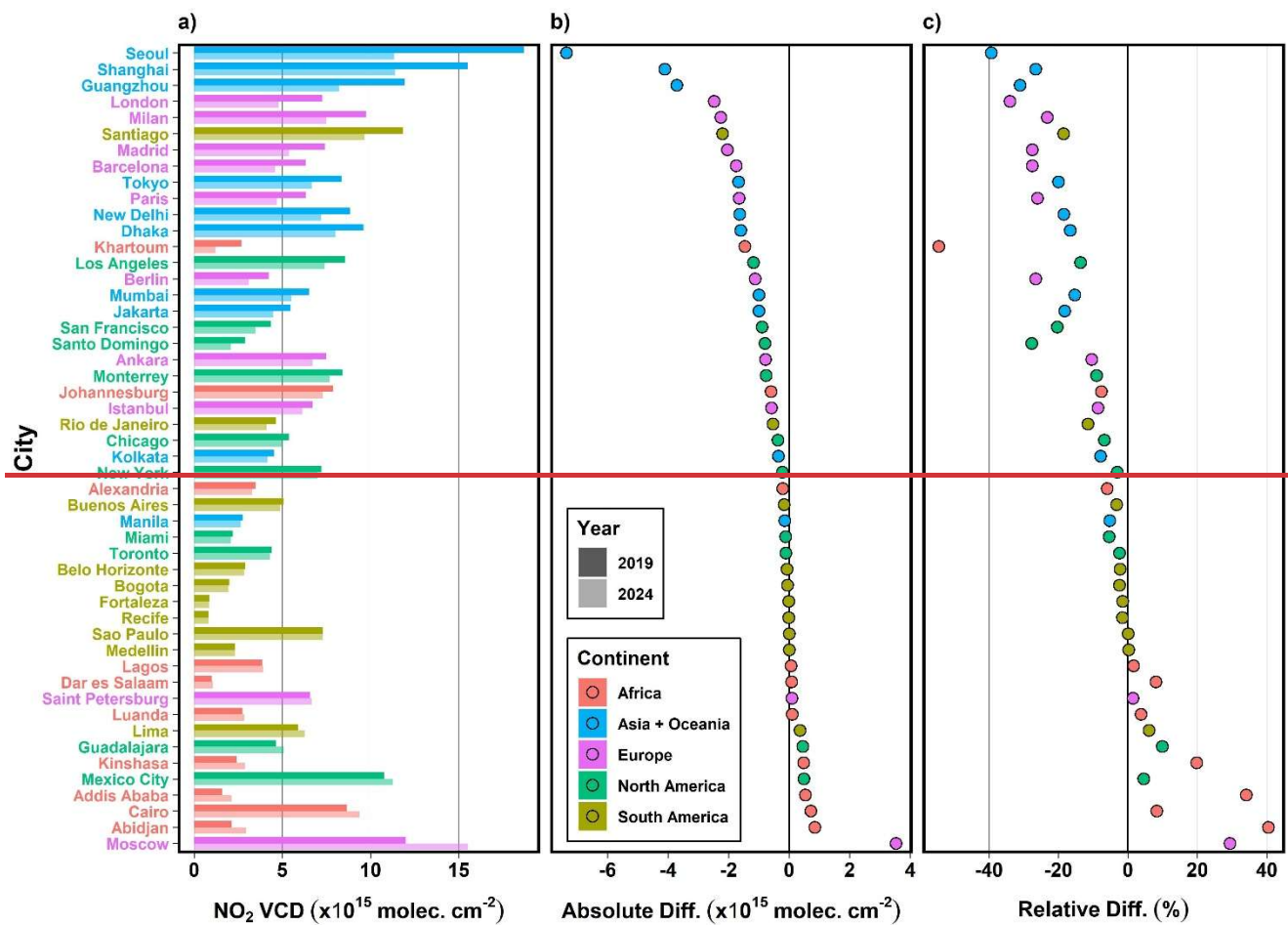
185 ~~similar bottom-up inventory, also provided at $0.1^\circ \times 0.1^\circ$ spatial resolution, but provides emissions estimates at the monthly~~
186 ~~level through the end of 2023. Uncertainties are inherent in such emissions are produced using a bottom-up method that~~
187 ~~combines activity data together inventories, with sector-specific a roughly 10-50% uncertainty when aggregating emissions~~
188 ~~factors to produce gridded annual emissions. Similar to the country level, and even larger uncertainty for individual grid points~~
189 ~~(Crippa et al., 2018).~~

190 Like the handling of TROPOMI data (Sec. 2.213), we use GHS-SMOD to quantify ~~mean~~annual NO_x emissions for each urban
191 cluster.

4 Urban-level NO₂ Global VCD trends from 2019 to 2024 in Major Urban areas

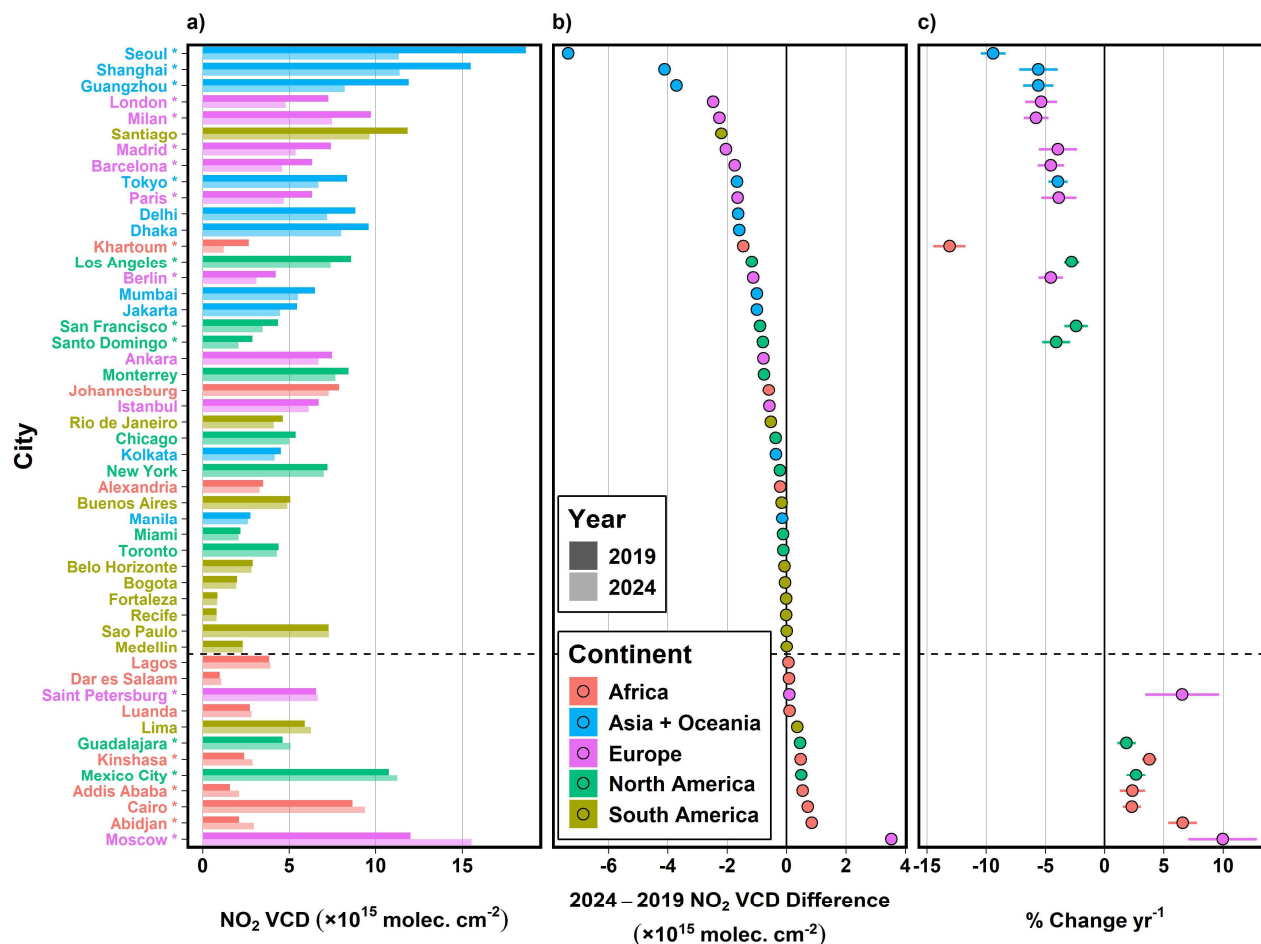
Using the method outlined in Section 2.2.1, the GHS-SMOD urban cluster boundaries are used to determine mean TROPOMI NO₂ concentrations for all urban clusters globally ~~with a minimum population of 50,000.~~ Of all 11,534 GHS-SMOD urban clusters, 58.1% are in Asia and Oceania, 18.5% are in Africa, 10.9% are in Europe, 6.2% are in North America and 6.3% are in South America. Looking at VCD changes from 2019 to 2024 in the 50 cities representing the ten most populous urban clusters on each continent, with Asia and Oceania considered jointly, East Asian cities represent four and European cities represent five of the ten largest VCD decreases (Fig. 7a2a). Seoul experienced the greatest absolute reduction in annual mean NO₂ VCD of any of these 50 cities, ~~with annual average levels from 2019 to 2024 (Fig. 2b), representing a significant~~ decreasing ~~by 7~~trend of -9.4×10^{15} molecules cm⁻² (Fig. 7b), or nearly -40% ($\pm 1.0\%$ yr⁻¹ ($p < 0.001$; Fig. 7e2c). London, England produced the greatest NO₂ VCD decrease of the ten most populous European cities, ~~with a mean decrease of 2. (-5×10^{15} molecules cm⁻² (Fig. 7b), or -34%. This decrease occurred $4 \pm 1.3\%$ yr⁻¹; $p < 0.001$), occurring~~ alongside the introduction of the city's ultra-low emission zone introduced in 2019 and expanded in 2023, which has ~~been shown~~contributed to ~~decreased~~decreased local NO₂ concentrations (Hajmohammadi and Heydecker, 2022).

~~Large~~ None of the ten largest South American cities ~~generally~~ experienced ~~minimal changes~~ a statistically significant trend in NO₂ VCD, with relative changes typically less than $\pm 5\%$ 0.6×10^{15} molecules cm⁻² (Fig. 7e2b). The most notable exception is Santiago, Chile, which experienced ~~an annual~~ mean VCD ~~decrease~~difference of nearly ~~20% from 2.2×10^{15} molecules cm⁻² between 2019 to and 2024.~~ The Of the largest North American cities ~~mostly experienced moderate VCD decreases, with the largest absolute decreases occurring, significant decreasing trends occurred~~ in Los Angeles (~~-13.7%~~) $2.8 \pm 0.6\%$ yr⁻¹; $p = 0.004$), and the San Francisco Bay Area (~~-20.4%~~), ~~and largest increases occurring~~ $2.8 \pm 0.6\%$ yr⁻¹; $p = 0.023$), while ~~significant increasing trends occurred~~ in the Mexican cities of Guadalajara (~~+1.9.9%~~) $\pm 0.8\%$ yr⁻¹; $p = 0.019$) and Mexico City (~~+4.6%~~). ~~Chicago and New York City, two of the largest cities in the U.S., also experienced decreases, though less pronounced.~~ $2.7 \pm 0.8\%$ yr⁻¹; $p = 0.010$).



214

215

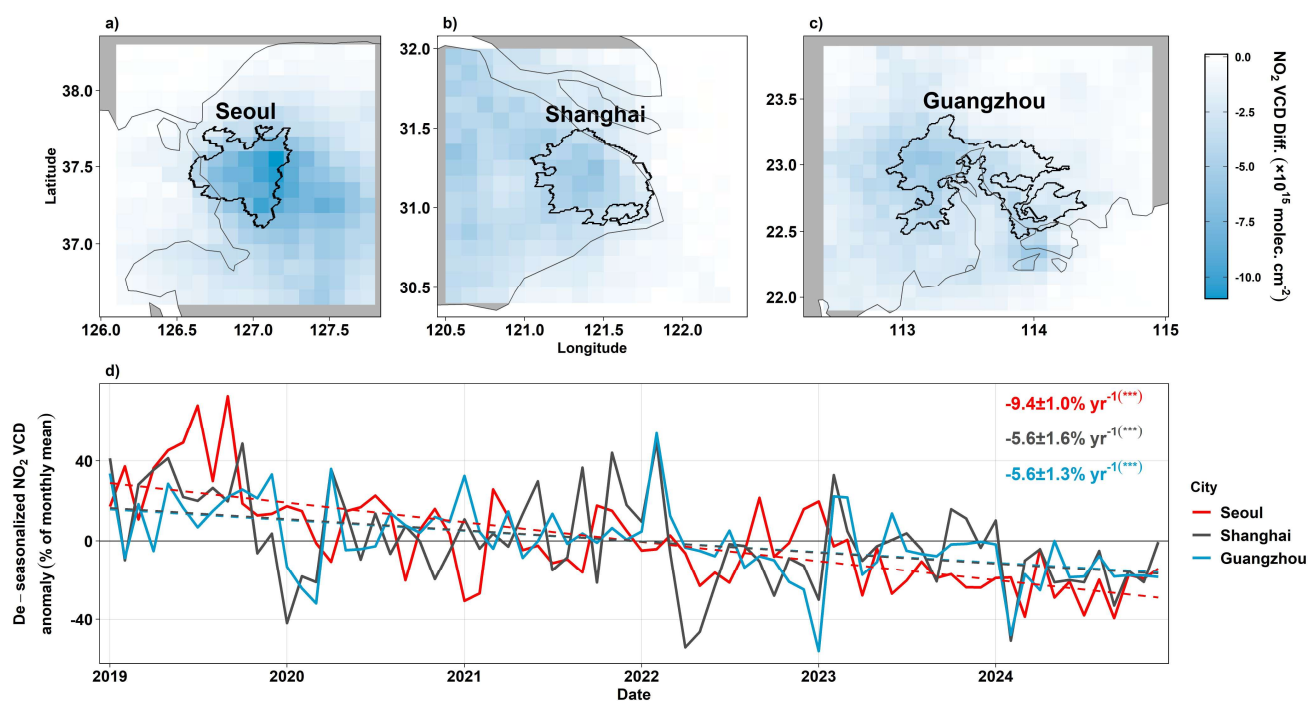


216

217 Figure 72: (a) NO₂ VCD in 2019 (dark bars) and 2024 (light bars) for the 10 most populous urban clusters on each continent, based
 218 on GHS-SMOD populations. (b) Absolute difference in NO₂ VCD for each city from 2019 to 2024. (c) Relative NO₂ VCD trend in
 219 units of percent change in VCD yr⁻¹ from 2019 to 2024. Horizontal bars represent standard error associated with the trend analysis.
 220 Colors correspond to the respective continent for each city. Cities are ordered by magnitude of absolute VCD decrease. Statistically
 221 significant trends are denoted with an asterisk by each city name. Only statistically significant trends are reported in panel c.

222 Most of the largest African cities experienced increased NO₂ VCDs from 2019 to 2024, with Abidjan, Ivory Coast experiencing
 223 the largest urban increase of $+6.6 \pm 1.2\% \text{ yr}^{-1}$; $p < 0.85 \times 10^{-15}$ molecules cm^{-2} (Fig. 7b), or an increase of 40.5% (Fig. 7c).
 224 Additional notable African increases are occurring in Cairo, Egypt ($+82.3\%$); $\pm 0.8\% \text{ yr}^{-1}$; $p = 0.006$); Addis
 225 Ababa, Ethiopia ($+34.1\%$); $2.4 \pm 1.1\% \text{ yr}^{-1}$; $p = 0.012$); and Kinshasa, DR Congo ($+19.9\%$). The largest decrease on the African
 226 continent was observed in $-3.8 \pm 0.6\% \text{ yr}^{-1}$; $p < 0.001$). In the Sudanese capital of Khartoum, which experienced an average
 227 decrease of 1.46×10^{15} molecules cm^{-2} (Fig. 7b) or a decrease of 54.5% (Fig. 7c). These strong VCD decreases NO₂ VCDs
 228 started decreasing in Khartoum coincide 2023, coinciding with the onset of conflict within Sudan (Guo et al., 2023; Fig. S10).
 229 This resulted in the country, causing large portions of the largest absolute NO₂ VCD decrease of any African city from 2019

230 to be displaced, impacting NO_2 concentrations (see Sec. 3.2).
 231 2024 (Fig. 2b), and a decreasing trend of $-13.1 \pm 1.4\% \text{ yr}^{-1}$ ($p <$
 232 0.001).
 233 Of the cities presented in Fig. 72, the three largest absolute decreases between 2019 and 2024 were in the East Asian cities of
 234 Seoul, South Korea (Fig. 8a,3a); Shanghai, China (Fig. 8b)3b); and Guangzhou, China (Fig. 8e)3c). Decreases in Seoul
 235 experienced decreases greater than 7×10^{15} molecules cm^{-2} from 2019 to 2024, largely due to effective coincide with known
 236 policies implemented by the South Korean government since the early 2000s to reduce local emissions, as well as
 237 trends changes in emissions that began following the COVID-19 pandemic (Ho et al., 2021; Seo et al. 2021). The observed
 238 annual decreases in these East Asian cities were primarily driven by decreases during the winter months (Fig. 7d). European
 239 cities also experienced some of the largest decreases in VCD, with the three largest decreases occurring in London, UK ($-$
 240 34%); Milan, Italy (-23%); and Madrid, Spain (-28%) (Fig. S8). Three cities with notable increases include Moscow, Russia
 241 ($+29\%$), Baghdad, Iraq ($+17\%$) and Riyadh, Saudi Arabia ($+13\%$) (Fig. S9). Moscow experienced the largest NO_2 VCD
 242 increase of any large GHS-SMOD city through 2024, with a mean increase of 3.5×10^{15} molecules cm^{-2} (Fig. 7b). The an
 243 increasing VCD trend in Moscow accelerated to $+9.97\% \text{ yr}^{-1}$ ($p=0.001$). This increase was accompanied by anomalously high
 244 monthly mean concentrations in early 2022 (Fig. S9S11), following the onset of the Russia-Ukraine war in Ukraine, when
 245 monthly mean NO_2 VCDs for March reached 59×10^{15} molecules cm^{-2} (see Sec. 3.3).



246
 247 **Figure 83:** Absolute change in mean annual NO_2 VCD from 2019 to 2024 for three East Asian cities: (a) Seoul, South Korea, (b)
 248 Shanghai, China and (c) Guangzhou, China. Colors in panels a-c show magnitude of VCD change, thin lines show national borders

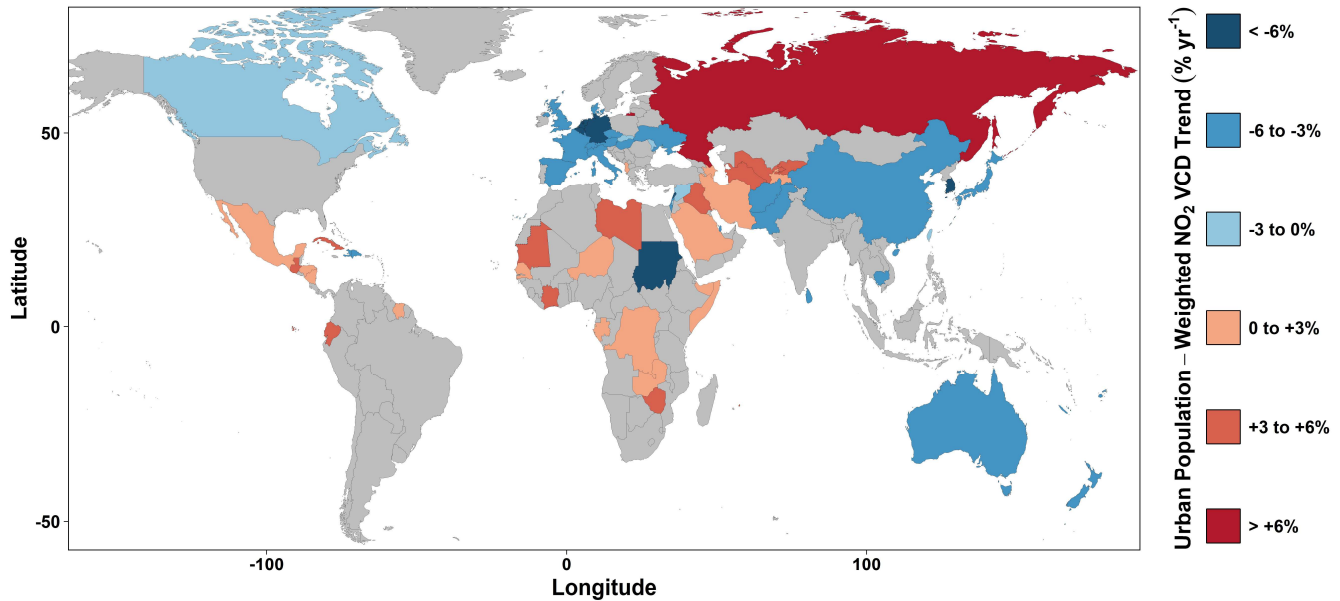
249
250
251
252

or coastlines, and thick lines show the GHS-SMOD urban boundary. (d) Solid lines show de-seasonalized monthly ~~mean TROPOMI~~ NO₂ VCD anomaly from 01/2019 through 12/2024, colored by city. Dashed lines ~~and equations show~~ represent ordinary least-squares regression trends, ~~with the slope representing the~~ The % change yr⁻¹, standard error and statistical significance of each trend is reported in NO₂ VCD per month, and the y-intercept representing the intercept for January, 2019 the top right of panel c.

253 **4 Population-Weighted country-level urban TROPOMI NO₂ trends**

254 Aggregating the NO₂ VCD changes to the country level ~~and taking into account~~ by considering the population of each urban
255 cluster (Eq. 1), ~~the urban and we identify~~ population-weighted VCD trends in countries globally (Fig. 4). The majority of urban
256 NO₂ VCD increases were observed in much of Central America including Mexico, in Africa, in the Middle East and in Central
257 Asia. Russia experienced the largest population-weighted VCD increase of $6.2 \pm 3.6\% \text{ yr}^{-1}$ ($p = 0.046$). Broad urban VCD
258 decreases were observed in numerous countries across Western and Central Europe, as well as Eastern Asian countries. The
259 largest urban population-weighted decrease occurred in South Korea ($-8.74 \pm 0.9\% \text{ yr}^{-1}$; $p < 0.001$).

260



261

262 **Figure 4: Global spatial representation of the urban population-weighted NO₂ VCD trend from 2019 to 2024. Gray fill denotes**
263 **countries with a statistically insignificant trend ($p > 0.05$)**.

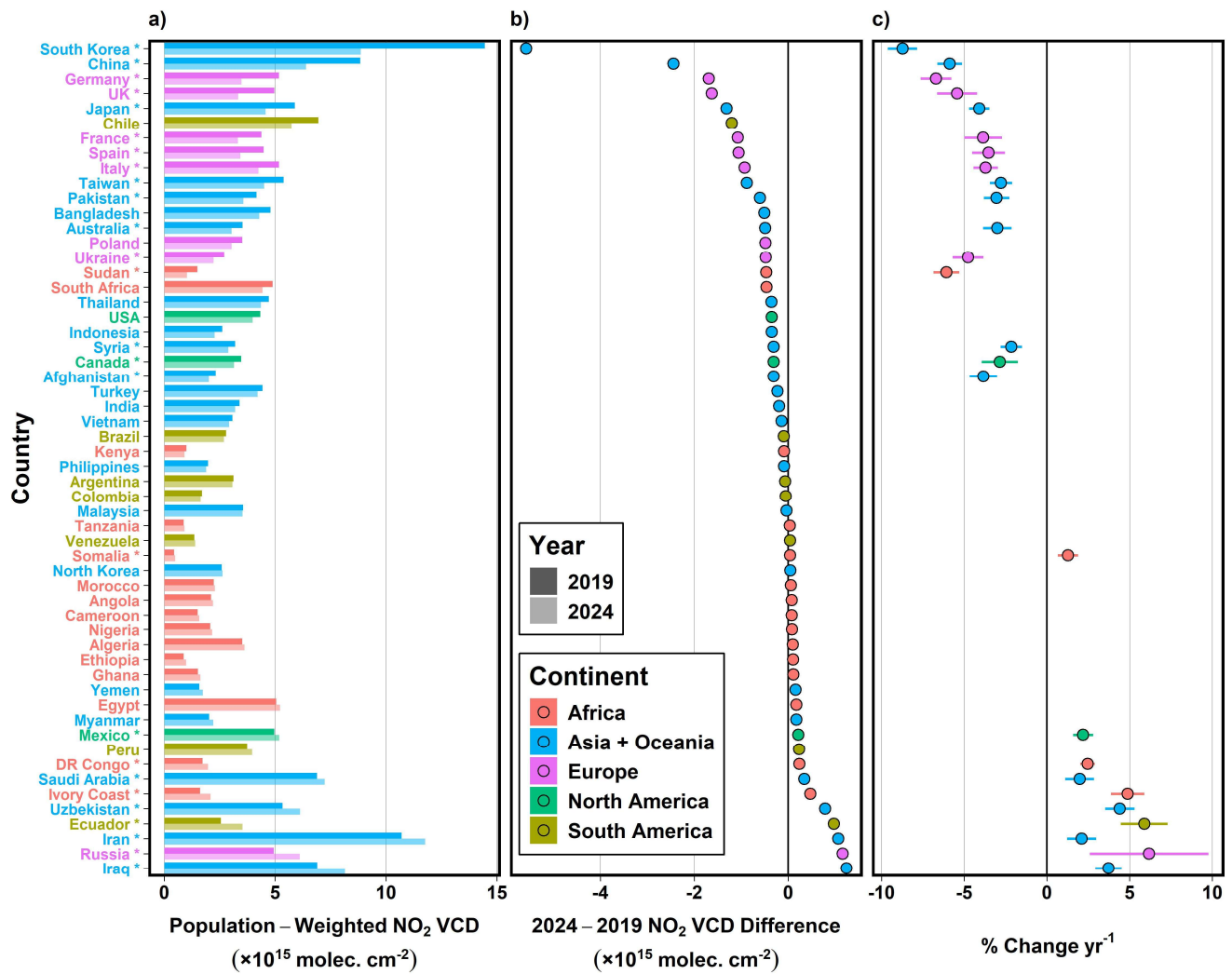
264 Much of the Middle East exhibited substantial increases in urban population-weighted NO₂ VCDs from 2019 to 2024, including
265 in Saudi Arabia ($+2.0 \pm 0.9\% \text{ yr}^{-1}$; $p = 0.009$), Iraq ($+3.7 \pm 0.8\% \text{ yr}^{-1}$; $p < 0.001$), and Iran ($+2.1 \pm 0.9\% \text{ yr}^{-1}$; $p = 0.013$), with broad
266 increases that extend beyond the urban environment. One of the most salient VCD decreases in the Middle East occurred in
267 Lebanon ($-8.5 \pm 1.0\% \text{ yr}^{-1}$; $p < 0.001$), coinciding with the country's severe economic and financial crisis that began in late 2019
268 (Harake et al., 2019). VCD decreases through 2024 were particularly stark in the Lebanese capital Beirut ($-7.9 \pm 1.1\% \text{ yr}^{-1}$;
269 $p < 0.001$). Additional Middle Eastern countries that exhibited decreased urban NO₂ VCDs through 2024 include much of Israel
270 ($-4.5 \pm 0.9\% \text{ yr}^{-1}$; $p < 0.001$), Qatar ($-3.4 \pm 1.2\% \text{ yr}^{-1}$; $p = 0.004$), and Afghanistan ($-3.8 \pm 0.8\% \text{ yr}^{-1}$; $p = 0.003$). Notable urban NO₂
271 VCD changes in less populated countries of Asia and Oceania include decreases in Cambodia ($-5.0 \pm 0.9\% \text{ yr}^{-1}$; $p < 0.001$), Sri

272 Lanka (-5.4±0.9% yr⁻¹; p<0.001) and Australia (-3.0±0.9% yr⁻¹; p=0.008). Urban increases were observed in much of Central
273 Asia, including Uzbekistan (+4.4±0.9% yr⁻¹; p<0.001) and Turkmenistan (+4.5±0.5% yr⁻¹; p<0.001).

274 NO₂ VCD decreases for more populous countries with an urban population of at least nine million were largest in ~~the~~ East
275 Asia, including ~~South Korea~~, China (-6.0±1.0% yr⁻¹; p < 0.001) and Japan, ~~as well as countries of Western and Central Europe~~
276 (-4.1±0.6% yr⁻¹; p < 0.001) (Fig. 405). Urban population-weighted VCD decreases in South Korea were particularly
277 pronounced, with ~~concentrations decreasing by a~~ population-weighted concentration difference of -5.6×10^{15} molecules cm⁻²
278 from 2019 to 2024. between 2019 and 2024. In South Asia, the neighboring countries of Afghanistan (-3.8±0.8% yr⁻¹; p=0.003)
279 and Pakistan (-3.0±0.8% yr⁻¹; p=0.012) exhibited some of the only country-level VCD decreasing trends for the region.
280 Significant decreases also occurred in numerous countries of Western and Central Europe, with Germany
281 experienced~~experiencing~~ the largest VCD decrease in Europe through 2024, with a decrease of 1.7×10^{15} molecules cm⁻².
282 in Europe through 2024 (-6.7±0.9% yr⁻¹; p < 0.001). Of the most-populous European countries, Russia was the only country to
283 experience increased population-weighted NO₂ VCDs through 2024.

284 A majority of larger African countries exhibited insignificant urban VCD changes, with 2024 population-weighted VCDs
285 changing by less than 0.25×10^{15} molecules cm⁻² relative to 2019 levels (Fig. 5b). Exceptions include larger changes in Sudan
286 (-6.1±0.8% yr⁻¹; p < 0.001) and Ivory Coast (+4.9±1.0% yr⁻¹; p < 0.001). Middle Eastern and Central Asian countries
287 experienced some of the largest urban VCD increases, with Iraq experiencing the largest difference between 2019 and 2024
288 levels of any larger country ($+1.2 \times 10^{15}$ molecules cm⁻²). Chile saw the largest ~~decreased~~ difference in annual mean urban NO₂
289 VCD between 2019 and 2024 of any South American country, due in large part to ~~VCD decreases~~ lower 2024 annual mean
290 NO₂ VCDs in the capital city of Santiago. (Fig. 5b).

291



292

293

294

295

Figure 105: UrbanSame as Fig. 2, but presenting changes and trends in country-level urban population-weighted NO₂ VCD changes from 2019 to 2024 VCDs for the 56 countries with an urban population of at least nine million, based on urban cluster populations provided from GHS-SMOD.

296 **3-Global⁵ Regional TROPOMI NO₂ vertical column densities from 2019 to 2024**

297 The following subsections describe the NO₂ VCDs and trends in ~~four~~^{five} global subregions: Asia and Oceania, Africa, Europe,
298 North ~~America~~ and South America.

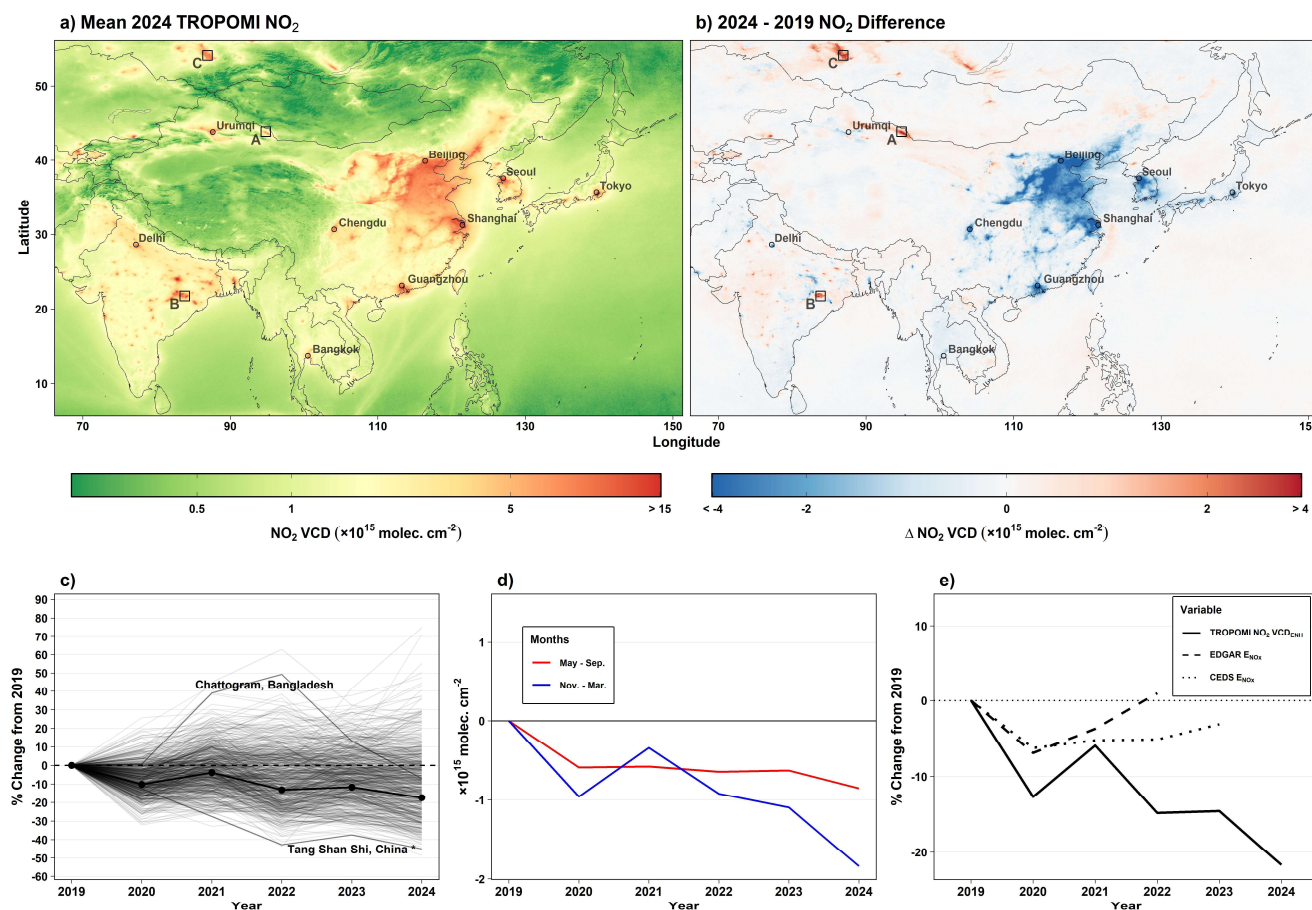
299 **3.5.1 Asia and Oceania**

300 North and East China, one of the most populated regions globally with approximately 11% of the 1000 largest GHS-SMOD
301 cities, produced the broadest continuous expanse of 2024 annual mean NO₂ VCDs at or above 5×10^{15} molecules cm⁻² (Fig.
302 ~~2a6a~~). Despite this, substantial VCD decreases were observed in this region from 2019 to 2024 (Fig. ~~2b~~). ~~While~~^{6b}. NO₂
303 concentrations had already been decreasing in China prior to 2019 (Liu et al., 2016; de Foy et al., 2016), and the decrease
304 ~~accelerated~~^{continued} after the onset of the COVID-19 pandemic, ~~coinciding with reduced emissions~~ during which numerous
305 lockdowns throughout the country ~~from between~~ 2020 ~~to~~ and 2022 led to reduced NO₂ concentrations (Zheng et al., 2021;
306 Cooper et al., 2022; Levelt et al., 2022; Ma et al., 2023; Zhao et al., 2024). The decrease in NO₂ also coincided with general
307 Chinese government policies directed at reducing emissions, including stricter emissions controls for industrial sources, energy
308 generation and the transportation sector (Shi et al., 2022; Li et al., 2024). ~~Few regions in China experienced increased VCDs,~~
309 ~~with the most notable increases occurring outside of major urban areas. The most substantial increase in VCD over China~~
310 ~~through 2024 was observed in the sparsely populated Santanghu Basin (Fig. 3a), a region in eastern Xinjiang Province with a~~
311 ~~relatively nascent coal-mining industry (Zhang et al., 2018; Liu et al., 2018). Annual mean NO₂ VCDs in the basin increased~~
312 ~~by 1.9×10^{15} molecules cm⁻², or +172%, from 2019 to 2024. The expansion of mining operations is clearly evident in visible~~
313 ~~satellite imagery (Fig. S3).~~

314 In India, ~~elevated~~^{the largest differences in urban NO₂ VCD between 2019 and 2024 were observed in Delhi (-1.6×10^{15}}
315 ~~molecules cm⁻²) and Mumbai (-1.0×10^{15} molecules cm⁻²), though neither city exhibited statistically significant decreasing~~
316 ~~trend over that period. Elevated~~ NO₂ near numerous coal-fired power plants and coal mines is a common feature in India
317 (Panda et al., 2023), evidenced by the many apparent point sources in the 2024 annual average TROPOMI VCDs throughout
318 the country (Fig. ~~4a6a~~). NO₂ VCDs increased at many of these points sources from 2019 to 2024 (Fig. ~~4b6b~~), suggesting an
319 increase in emissions from energy production and use. In the Middle Eastern countries East and Central Asia, urban regions
320 experienced some of the highest NO₂ VCDs globally in the TROPOMI record. Near the (Fig. 7). The Iranian capital of Tehran,
321 2024 by far has the largest annual average NO₂ VCDs of individual grid cells exceeded 40×10^{15} molecules cm⁻² (Fig. 4a),
322 the highest urban annual average among VCD in the TROPOMI tropospheric NO₂ record for all global GHS-SMOD cities.
323 Much of the Middle East exhibited substantial increases in population-weighted, urban NO₂ VCDs from 2019 to 2024, most
324 notably in regions of Saudi Arabia (+5%), Iraq (+18%), and Iran (+10%), with broad increases that extend beyond the urban
325 environment. One of the most salient VCD decreases in the Middle East occurred in Lebanon (-39%), coinciding with the
326 country's severe economic and financial crisis that began in late 2019 (Harake et al., 2019). VCD decreases through 2024 were

327 particularly stark in the Lebanese capital Beirut (-6.7×10^{15} molecules cm^{-2} ; -37%). Additional Middle Eastern countries that
 328 exhibited decreased urban NO_2 VCDs through 2024 include much of Israel (-27%), Kuwait (-5%), Qatar (-17%), and
 329 Afghanistan (-13%), with annual mean values remaining above 30×10^{15} molecules cm^{-2} throughout the entirety of the
 330 TROPOMI record (Fig. S12).

331



332

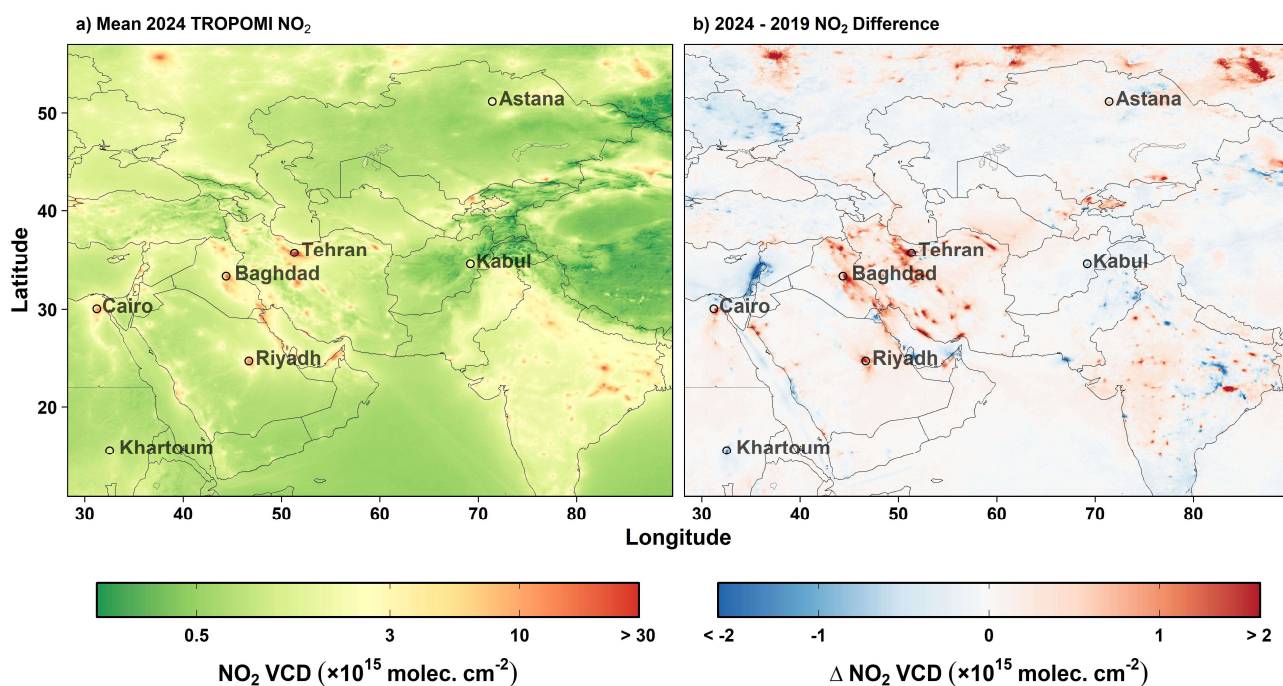
333 **Figure 46:** Same as Fig. 2, but centered on the Middle East. Labeled black squares indicate the locations of mining regions highlighted
 334 in Fig. 3.

335 **3:** (a) Mean 2024 TROPOMI NO_2 VCDs and (b) relative difference in annual mean TROPOMI VCDs between 2019 and 2024,
 336 centered on South and East Asia. Regions A, B and C represent the Santanghu Basin, the Ib Valley and Kuzbass mining regions,
 337 respectively, as highlighted in Fig. 12. (c) Population-weighted percent difference in annual mean TROPOMI NO_2 VCD relative to
 338 2019 levels for all GHS-SMOD urban clusters in Asia and Oceania (solid black line), and percent change in VCD for individual
 339 clusters with a population of at least 500,000 (gray lines). Asterisks denote a significant trend. (d) Absolute population-weighted
 340 difference in VCD for urban clusters in Asia and Oceania in May-September (red line) and November to March (blue line). (e)
 341 Relative difference in population-weighted TROPOMI NO_2 urban enhancement (VCD_{ENH} ; solid line, 2019-2024), NO_x emissions
 342 from the EDGARv8.1 emissions inventory (dashed line, 2019-2022) and CEDS emissions inventory (dotted line, 2019-2023).

343 Across Asia and Oceania as a whole, which contain a majority of all urban clusters globally, population-weighted NO₂ VCDs
344 were approximately 17% lower in 2024 than in 2019 (Fig. 6c). One notable decrease in Asia occurred in the Chinese city of
345 Tangshan Shi, located to the east of Beijing, which experienced an NO₂ VCD decrease of nearly 45% from 2019 to 2024. The
346 largest increase in Asia through 2024 occurred in the Mongolian capital of Ulaanbaatar, where the 2024 mean VCD was more
347 than 70% larger than in 2019. Numerous Bangladeshi cities, including Chattogram, experienced substantially increased VCDs
348 from 2020 through 2022, with VCDs decreasing again by 2024 to the near 2019 levels (Fig. S13).

349 Different seasons can have outsize impact on the relative change in annual NO₂ VCD. In cities of Asia and Oceania, the bulk
350 of the observed annual decreases through 2024 occurred during November – March (Fig. 6d), with a population-weighted
351 decrease of -1.8×10^{15} molecules cm⁻². Although the absolute changes in November – March were larger than in May –
352 September, the relative percent changes for the two periods were more comparable (Fig. S14).

353



354

355 Figure 7: (a) Mean 2024 TROPOMI NO₂ VCDs and (b) relative difference in annual mean TROPOMI VCDs between 2019 and
356 2024, centered on the Middle East and Central Asia.

357 Urban NO₂ concentrations are not only influenced by local emissions, but also by advection of upwind pollutants into the urban
358 boundary. We account for the role that upwind background concentrations may play in urban NO₂ concentrations by identifying
359 changes in the urban enhancement of NO₂ (VCD_{ENH}), represented by the difference between NO₂ VCDs in the urban cluster
360 and the urban background VCD. By removing the background concentrations, we expect that the percent change in VCD_{ENH}

361 relative to a baseline year can be primarily attributed to changes in local, urban NO_x emissions. We then evaluate changes in
362 VCD_{ENH} against changes in gridded NO_x emissions inventories from (1) the EDGARv8.1, with data available through 2022
363 and (2) CEDS, with data available through 2023 (Fig. S15).

364 In Asia and Oceania, cities experienced sustained decreases in VCD_{ENH}, with population-weighted values 22.7% lower in 2024
365 than in 2019 (Fig. 6e). Cities in Asia and Oceania experienced VCD_{ENH} that tracked relatively well with both inventories from
366 2019 to 2021, with a mean difference of +4.0% (EDGARv8.1) and +3.6% (CEDS) between emissions and VCD_{ENH}. However,
367 in 2022, EDGARv8.1 showed increased emissions and CEDS exhibited mostly unchanged emissions, while VCD_{ENH} exhibited
368 a sharp decrease for that year. This resulted in a percentage difference of +15.8% (EDGARv8.1) and +9.7% (CEDS) between
369 emissions and VCD_{ENH} in 2022 relative to 2019 levels (Fig. 6e). The 2022 VCD_{ENH} decrease coincided with broad lockdowns
370 in China related to the COVID-19 pandemic, suggesting that EDGAR emissions may not reflect emissions decreases during
371 that lockdown period.

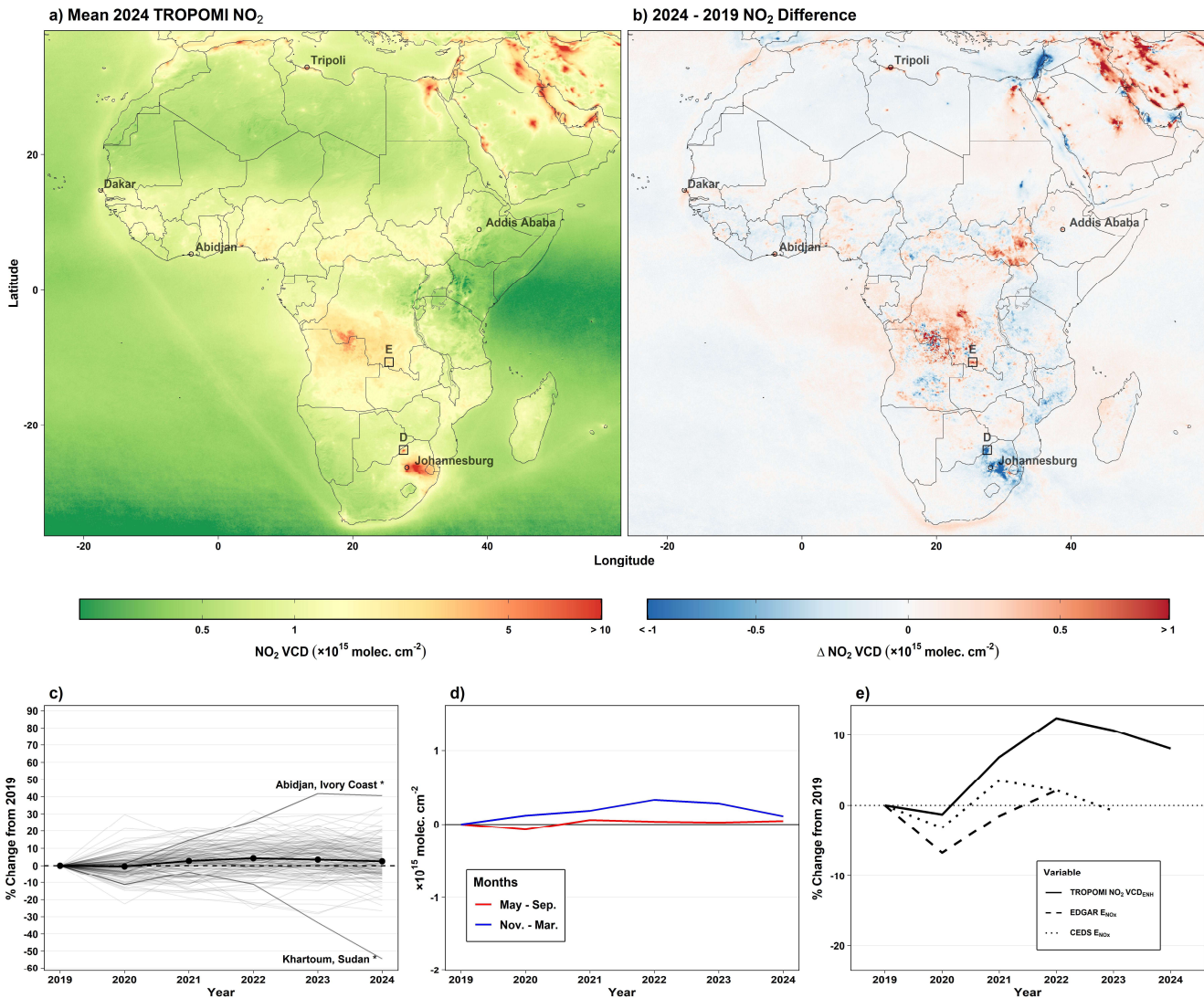
372 **5.2 Africa**

373 Areas to the east of Johannesburg, South Africa and the surrounding region exhibited the largest broadest enhanced NO₂ VCD
374 for the African continent in 2024 (Fig. S48a). Numerous surface coal mines and coal-fired power plants, particularly to the
375 east of Johannesburg, contribute to the region's NO₂ signature (Shikwambana et al., 2020). Despite these elevated NO₂ levels,
376 2024 mean NO₂ VCDs in the city of Johannesburg were 8% lower than in 2019. Northwest of Johannesburg in Limpopo
377 Province, mining operations at the Grooteegeluk surface coal mine, together with two adjacent power plants (Faure et al., 2010;
378 Shikwambana et al., 2020), produce one of the largest NO₂ point sources in Africa, despite annual mean NO₂ VCDs at the site
379 decreasing by 3.5×10^{15} molecules cm⁻² from 2019 to 2024, or a decrease of 32% (Fig. 3d). The Cairo, Egypt urban region, in
380 Northern Africa, represents the second largest Cairo, Egypt represents the largest urban NO₂ signature in Africa in 2024. The
381 2024 annual mean NO₂ VCD in Cairo was 9.4×10^{15} molecules cm⁻², and elevated VCDs extend along the Nile River south of
382 Cairo, as well as north into the Nile River Delta. Cairo exhibited increased VCDs from 2019 to of any major urban region in
383 Africa in 2024 (+8%), as did regions immediately adjacent to the Nile River, while regions north into the Nile River Delta
384 exhibited decreased NO₂ VCDs.

385 In the Sudanese capital of Khartoum, NO₂ VCDs started decreasing in 2023, coinciding with the onset of conflict within Sudan
386 (Guo et al., 2023). This resulted in annual mean VCDs decreasing by 58% from, when the annual mean NO₂ VCD reached 9.4
387 $\times 10^{15}$ molecules cm⁻². From 2019 to 2024 (Fig. S5). In a mining region known as the Copperbelt in the south of the Democratic
388 Republic of the Congo (DRC), broad NO₂ VCD increases were observed, including at a large surface mine near Kolwezi.
389 VCDs at the Kolwezi mine increased by 1.4×10^{15} molecules cm⁻² from 2019 to 2024, or an increase of 64% (Fig. 3e).
390 Numerous surface mines exist in the region, with most observing increases in NO_x emissions from mining operations in recent
391 years (Martínez-Alonso et al., 2023). Throughout the remainder of Africa, moderate VCD enhancements were observed near
392 most urban centers, with mean VCDs near most cities typically at or below 4×10^{15} molecules cm⁻² (Fig. 1a)., Cairo experienced

393 a statistically significant VCD increase of $2.3 \pm 0.8\% \text{ yr}^{-1}$ ($p = 0.006$). Along the African Mediterranean coast, most urban areas
394 showed increased NO_2 VCDs through 2024. ~~Other national capitals and major cities exhibited increased VCDs, including~~
395 ~~Abidjan, Ivory Coast (+41%); Addis Ababa, Ethiopia (+34%); Kinshasa, DRC (+20%); and Dakar, Senegal (+15%).~~
396 3Through 2024, African cities experienced a gradual increase in population-weighted NO_2 VCD (Fig. 8c). The largest percent
397 increase occurred in Abidjan, the capital city of Ivory Coast, which experienced an increase in NO_2 VCD of more than 40%
398 from 2019 through 2024. Khartoum, Sudan experienced the largest percent decrease of any large African City, with mean 2024
399 levels nearly 60% lower than in 2019.
400 In African cities (Fig. 8d), population-weighted VCDs during November-March were 0.1×10^{15} molecules cm^{-2} larger in 2024
401 than 2019, with little to no change occurring on average during May – September. When evaluating changes in VCD_{ENH} in
402 African cities, population-weighted VCD_{ENH} were +8.1% larger in 2024 relative to 2019 levels (Fig. 8e). One distinct feature
403 for African cities is the lack of a pronounced decrease in VCD_{ENH} during 2020, coinciding with the onset of the COVID-19
404 pandemic, a feature observed on all other continents. Evaluating trends in NO_x emissions inventories in African cities, we find
405 a mean difference of -8.0% (EDARv8.1) and -6.7% (CEDs) between inventory NO_x emission trends and VCD_{ENH} trends,
406 indicating a potential underestimate in both emissions inventories in African cities for this period.

407

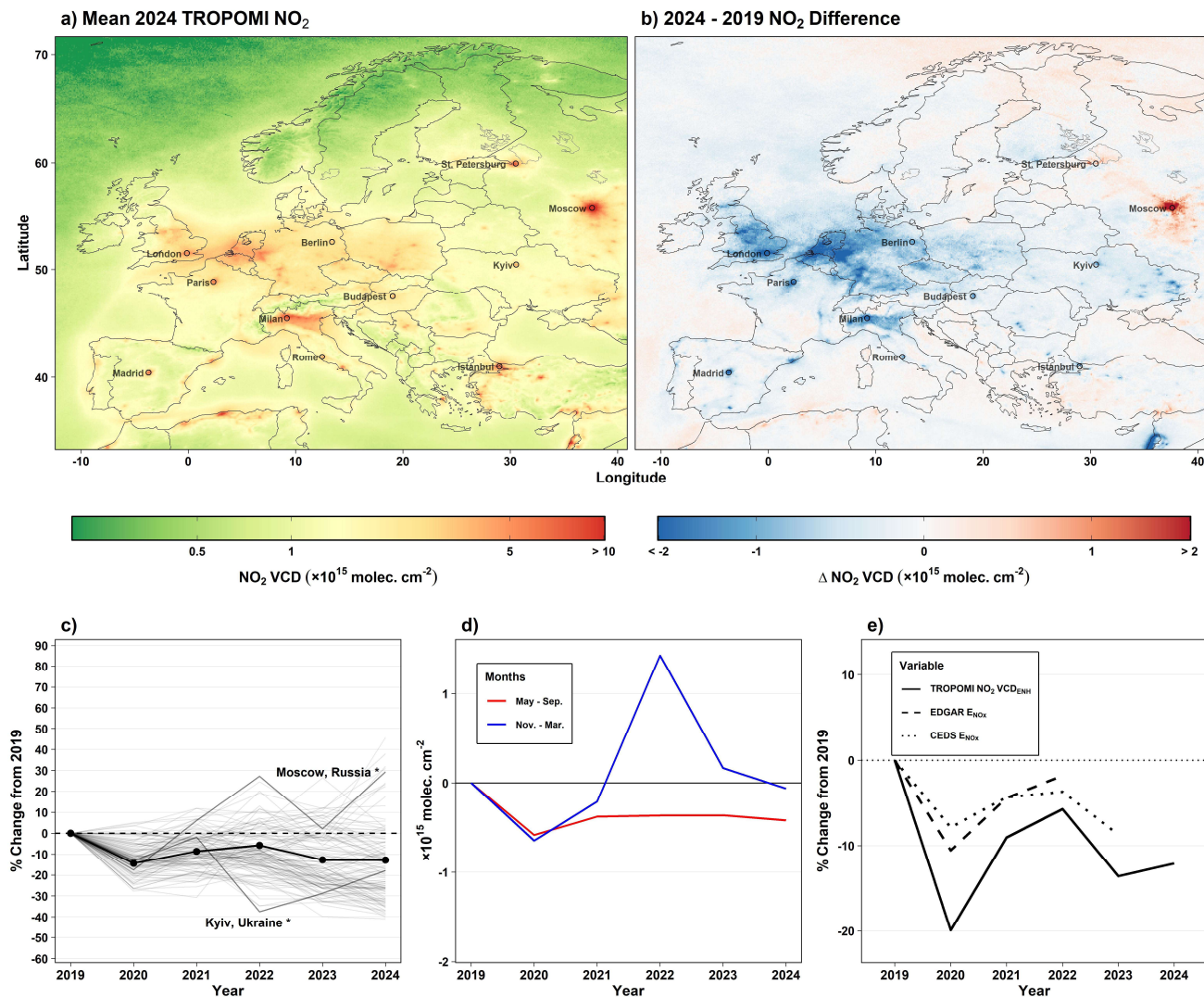


408

409 **Figure 8: Same as Fig. 6. but for the African continent. Regions D and E in panels a and b represent the Grootegeluk and Kolwezi**
 410 **mines, respectively, as highlighted in Fig. 12.**

411 **5.3 Europe**

412 NO₂ VCDs in Europe were largest in urban areas, with the largest 2024 mean VCD occurring in Moscow, Russia (15.5 ~~x~~ 10¹⁵
 413 molecules cm⁻²) (Fig. 5a9a). Broad enhanced 2024 annual mean VCDs exceeding 4 ~~x~~ 10¹⁵ molecules cm⁻² were observed in
 414 a region encompassing Belgium, the Netherlands and western portions of Germany, with values exceeding 5 ~~x~~ 10¹⁵ molecules
 415 cm⁻² in the Po River Valley of northern Italy.



417

418

Figure 9: Same as Fig. 6, but for Europe.

419

Of the 1257 urban clusters in Europe, All cities, 1007 (80%) exhibited lower VCDs in 2024 than in 2019. Of the 53 European urban clusters with a population greater than 1,000,000 experienced decreases, 2024 VCDs were lower than 2019 VCDs in 48 (91%), with the exception of Moscow (+29%) and other cities of western Russia, which experienced increases (Fig. 5b9b).

422

The broad decreases across large European cities are likely due to a combination of (1) continued decreased emissions trends that accelerated during continued following the COVID-19 pandemic, (2) continued transition to alternative energy sources following the start of the Russia-Ukraine war in 2022 and (3) existing policies implemented within the EU (Matthias et al., 2021; Rokicki et al., 2023; Cifuentes-Faura, 2022). These policies include the European Green Deal and European

425

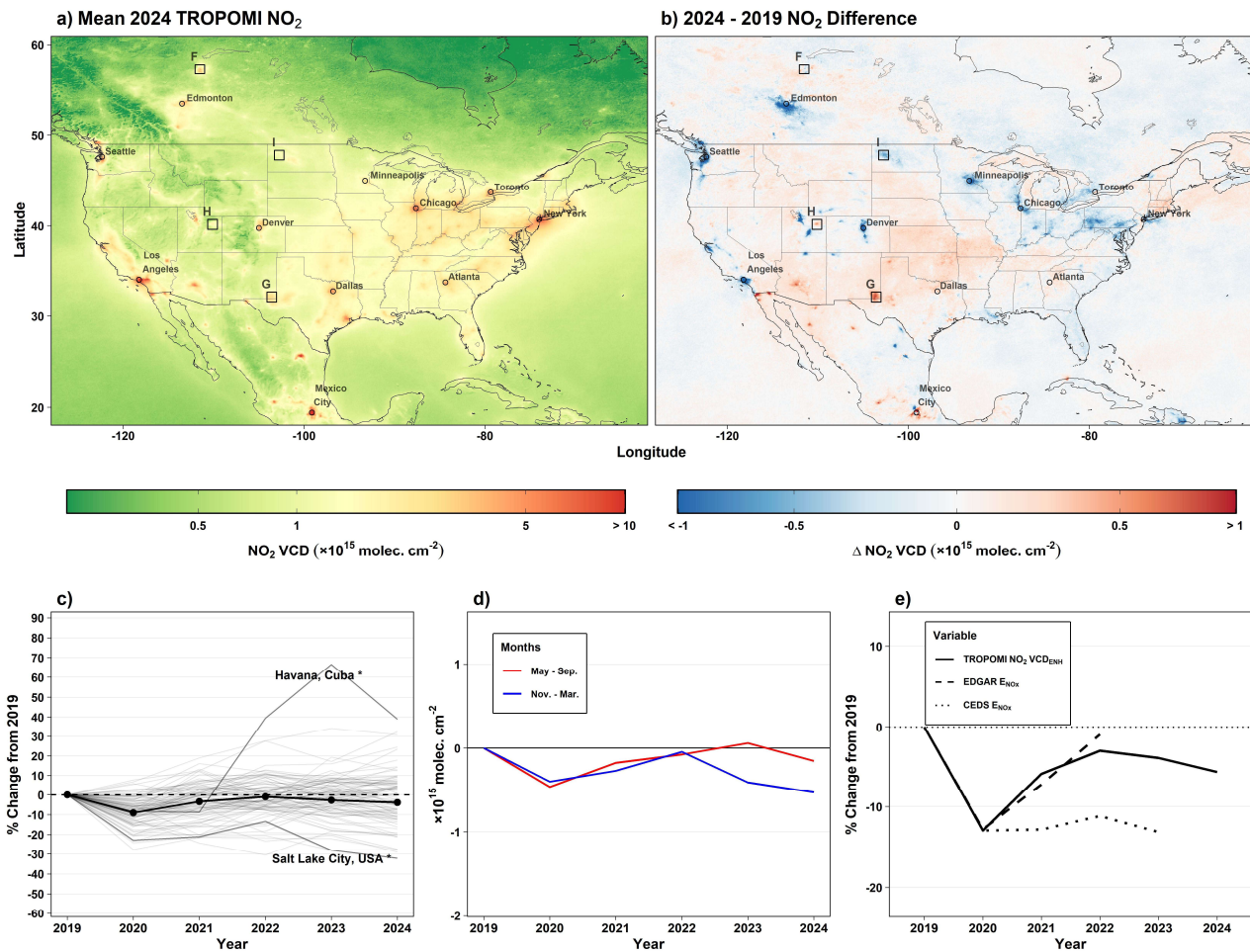
426 Climate Law, which promote zero-emission vehicles, stricter vehicle emissions targets and updated industrial emissions
427 regulations.

428 European cities experienced the most pronounced decrease in column NO₂ of any continent in 2020, with population-weighted
429 VCDs decreases by 16% from 2019 to 2020 (Fig. 9c). Previous work has attributed such decreases to the COVID-19 pandemic
430 (Cooper et al., 2022; Levelt et al., 2022). NO₂ VCDs rebounded marginally in 2021 and 2022, followed by decreases into 2023
431 and 2024. Decreases are more pronounced when only analyzing cities in the 27 member countries of the European Union (Fig.
432 S16). One notable feature within the European annual average VCDs is the contrasting VCD trends in Russian and Ukrainian
433 cities in 2022, at the onset of the Russia-Ukraine War (Fig. S17). In the Ukrainian capital of Kyiv, annual VCDs dropped
434 nearly 40% in 2022 relative to 2019, coinciding with a large portion of the city fleeing due to conflict in and near the city. To
435 contrast this, VCDs increased nearly 30% in the Russian capital of Moscow during the same period. Following 2022, VCDs
436 in Kyiv increased steadily, while in Moscow, levels decreased in 2023 then increased again in 2024.

437 Population-weighted May – September VCDs decreased by 0.4×10^{15} molecules cm⁻² (-10%) through 2024, while VCD
438 behavior during November – March has been less consistent, despite a sharp increase in winter-time levels in 2022 during the
439 onset of the Russia-Ukraine war (Fig. 9d). We note that the seasonal trends in Europe show more comparable winter and
440 summer changes if evaluating trends with Russian cities removed (Fig. S18). When accounting for background concentrations,
441 VCD_{ENH} in European cities experienced the largest drop in 2020 of any continent, with population-weighted VCD_{ENH}
442 decreasing by -20% from 2019 to 2020 (Fig. 9e). While both EDGARv8.1 and CEDS exhibited similar mean year to year
443 variability as VCD_{ENH} in European cities, trends in the inventories appeared underestimated, with each inventory estimate
444 exhibiting a mean percent difference relative to VCD_{ENH} of +6.0 and +5.9%, respectively. This suggests a slight underestimate
445 in decreasing emissions inventory trends in European cities relative to observed VCD_{ENH} levels.

446 **5.4 North America and South America**

447 Throughout North America, 2024 annual mean NO₂ VCDs were largest in urban regions, including Los Angeles (7.4×10^{15}
448 molecules cm⁻²), New York (7.0×10^{15} molecules cm⁻²), ~~Chicago (5.0×10^{15} molecules cm⁻²),~~ and Mexico City (11.3×10^{15}
449 ~~molecules cm⁻²) and Toronto (4.3×10^{15} molecules cm⁻²),~~ as well as near fossil fuel-fired power plant and mining operations
450 (Fig. 6a). ~~A majority of~~10a). ~~Most major~~ cities in the U.S. and Canada exhibited decreased or unchanged NO₂ VCDs (Fig. 6b),
451 ~~with notable exceptions being~~10b). Phoenix, Arizona (~~was one notable exception to these decreases, with mean 2024 VCDs~~
452 ~~10%) and Dallas, Texas (+6%), which experienced increases% higher than in 2019 (Fig. S6S19).~~



453

454 **Figure 10: Same as Fig. 6, but for North America. Regions F, G, H and I in panels a and b represent the Athabasca, Permian, Bakken**
 455 **and Uintah, respectively, as highlighted in Fig. 12.**

456 In Canada, the largest difference in VCD decreases were observed between 2024 and 2019 occurred in Alberta Province in and
 457 around Edmonton (-19%)- 0.9×10^{15} molecules cm^{-2} ; Fig. 10b), although the city did not experience a statistically significant
 458 trend for that period. In the U.S., aside from decreases in urban environments, the largest changes were observed in remote
 459 areas near coal power plants with reduced activity, e.g. near the decommissioned Navajo Generating Station in northern
 460 Arizona, the Four Corners Generating Station in northern New Mexico, and the Hunter and Huntington Power Plants in central
 461 Utah (Goldberg et al., 2021). Oil, gas, and coal-mining operations influenced regional VCD changes as well, with annual mean
 462 NO_2 VCDs decreasing from 2019 to 2024 in the Athabasca oil sands (+1%) in Northern Alberta (Fig. 3f), increases in the
 463 Permian (+29%) and Uintah (+35%) Basins in the southwestern U.S. (Fig. 3g-h), and decreases in the Bakken (-16%) in North
 464 Dakota (Fig. 3i). Apparent within the U.S. is a slight increase in background concentrations in rural regions, particularly in the

465 Central and Western U.S. It is unclear if this is due to an extension of the NO₂ lifetime due to decreasing VOCs and O₃ over
466 this 6-year period (e.g., Laughner & Cohen 2019) or due to increased NO_x emissions in rural areas or both. Further work
467 should investigate this.

468 In Mexico, Central America and the Caribbean, the largest VCDs are observed near Mexico City (11.3×10^{15} molecules cm⁻²)
469 and Monterrey, Mexico (7.7×10^{15} molecules cm⁻²), with numerous other notable urban signatures. (Fig. 10a). The largest
470 urban increases were observed at sites in Northern Mexico, including Mexicali (~~+31%~~) $6.1 \pm 0.9\%$ yr⁻¹; $p < 0.001$) and
471 Hermosillo (~~+32%~~) ~~as well as a handful of regions with decreased VCDs in northern Mexico, including Monterrey (-9%).~~
472 ~~VCDs also decreased near~~ $5.2 \pm 0.7\%$ yr⁻¹; $p < 0.001$). Additional notable changes occurred in the capital city of Santo Domingo,
473 Dominican Republic (~~-28%~~) $4.1 \pm 1.2\%$ yr⁻¹; $p = 0.006$), and ~~increased near~~Havana, Cuba (~~+39%~~) $11.2 \pm 1.7\%$ yr⁻¹; $p < 0.001$)
474 (Fig. 10b).

475 ~~In South America, the largest VCDs are observed~~Most North American cities experienced a decrease in annual NO₂ VCD of
476 less than 10% in 2020, with concentrations generally rebounding to 2019 levels by 2024 (Fig. 10c). Havana, Cuba was a
477 notable exception of North American cities, with VCDs increasing by nearly 70% through 2023 relative to 2019, with a slight
478 decrease in 2024. Cities in the western U.S., such as Salt Lake City and Denver experienced some of the largest percent
479 decreases on the continent, decreasing by approximately 30% through 2024. The bulk of the observed annual decreases through
480 2024 in North American cities occurred during winter (Fig. 10 d), with an average winter decrease of -0.5×10^{15} molecules
481 cm⁻² during those months. In North America, VCD_{ENH} decreased by 13% from 2019 to 2020 (Fig. 10e), compared with a
482 decrease of 10% in overall urban VCD from 2019 to 2020, and VCD_{ENH} remained approximately 7.5% below 2019 levels by
483 2024. Averaged for North America, population-weighted EDGAR NO_x emissions and VCD_{ENH} exhibited a similar change
484 relative to 2019 levels through 2022, with a mean difference of +0.3%, while CEDS and VCD_{ENH} exhibited a larger mean
485 difference of -6.1%, with differences most pronounced after 2020. This suggests relatively good agreement between North
486 American EDGAR and TROPOMI trends, while CEDS emissions for the region may be underestimated from 2020 onward
487 (Fig. 10e).

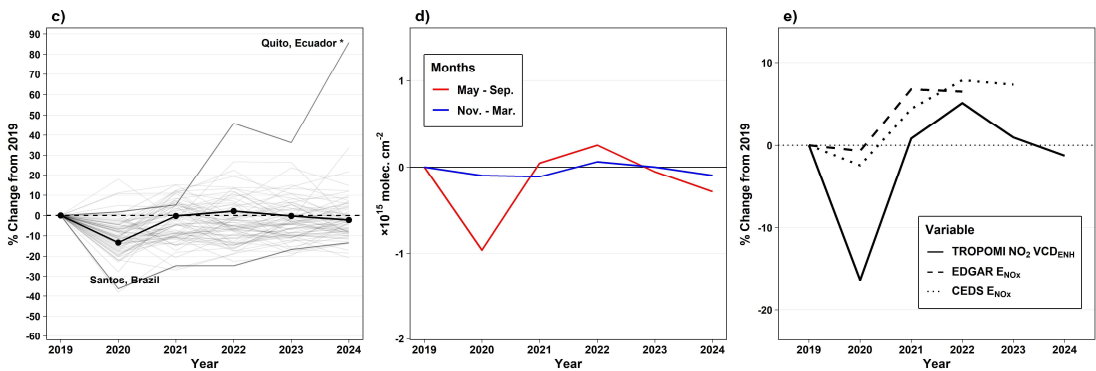
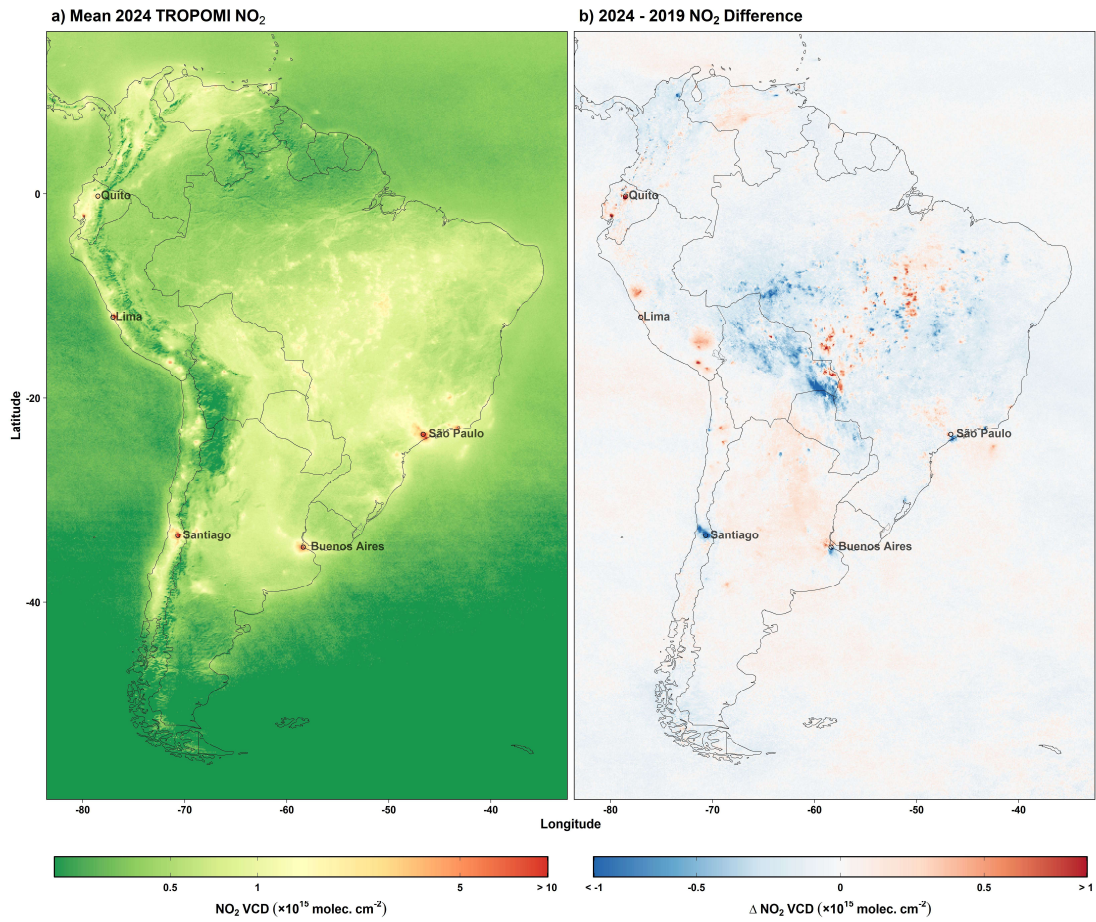
488 5.5 South America

489 The largest 2024 mean VCDs in South America are observed in urban regions, including near Lima, Peru (6.3×10^{15} molecules
490 cm⁻²); Santiago, Chile (9.7×10^{15} molecules cm⁻²); and Sao Paulo, Brazil (7.3×10^{15} molecules cm⁻²) (Fig. S711a). Regions
491 near Santiago experienced some of the largest ~~decreases~~differences in VCD in South America (~~-19%~~),between 2019 and 2024
492 (Fig. 11b) (-2.2×10^{15} molecules cm⁻²), while Quito, Ecuador experienced ~~the largest increase (+86%)~~a significant increasing
493 trend for that period ($+12.7 \pm 1.9\%$ yr⁻¹; $p < 0.001$).

494 South American cities experienced a 10% population-weighted VCD decrease in 2020, with mean concentrations rebounding
495 to 2019 values by 2021 and remaining around those levels through 2024 (Fig. 11ce). One notable exception is Quito, Ecuador,
496 which experienced a VCD increase of over 85% through 2024. Santos, Brazil, an active port town southeast of São Paulo,

497 experienced one of the largest VCD decreases in South America, with a 35% decrease in VCDs from 2019 to 2020, followed
498 by sustained, gradual annual increases through 2024.

499 Seasonal changes impacted South American cities less than cities on other continents through 2024 (Fig. 11d), with mean
500 winter and summer VCDs both changing by less than 0.3×10^{15} molecules cm^{-2} through 2024. Accounting for urban
501 background concentrations, South American cities experienced a population-weighted VCD_{ENH} decrease of 16% from 2019 to
502 2020, with concentrations rebounding to near 2019 levels by 2021 (Fig. 11e). Both EDGAR and CEDS estimated similar
503 population-weighted NO_x emissions trends for the region, though neither inventory appeared to capture the robust 2020
504 decrease observed by TROPOMI (Fig. 11e). Both inventories experienced a similar mean difference between emissions and
505 VCD_{ENH} (+7.7% and +6.7%, respectively), suggesting that urban NO_x emissions in both inventories may be overestimated for
506 the region.



507

508
509

Figure 611: Same as Fig. 26, but for North America. Squares and numbers represent select oil and gas regions highlighted in Fig. 3. South America.

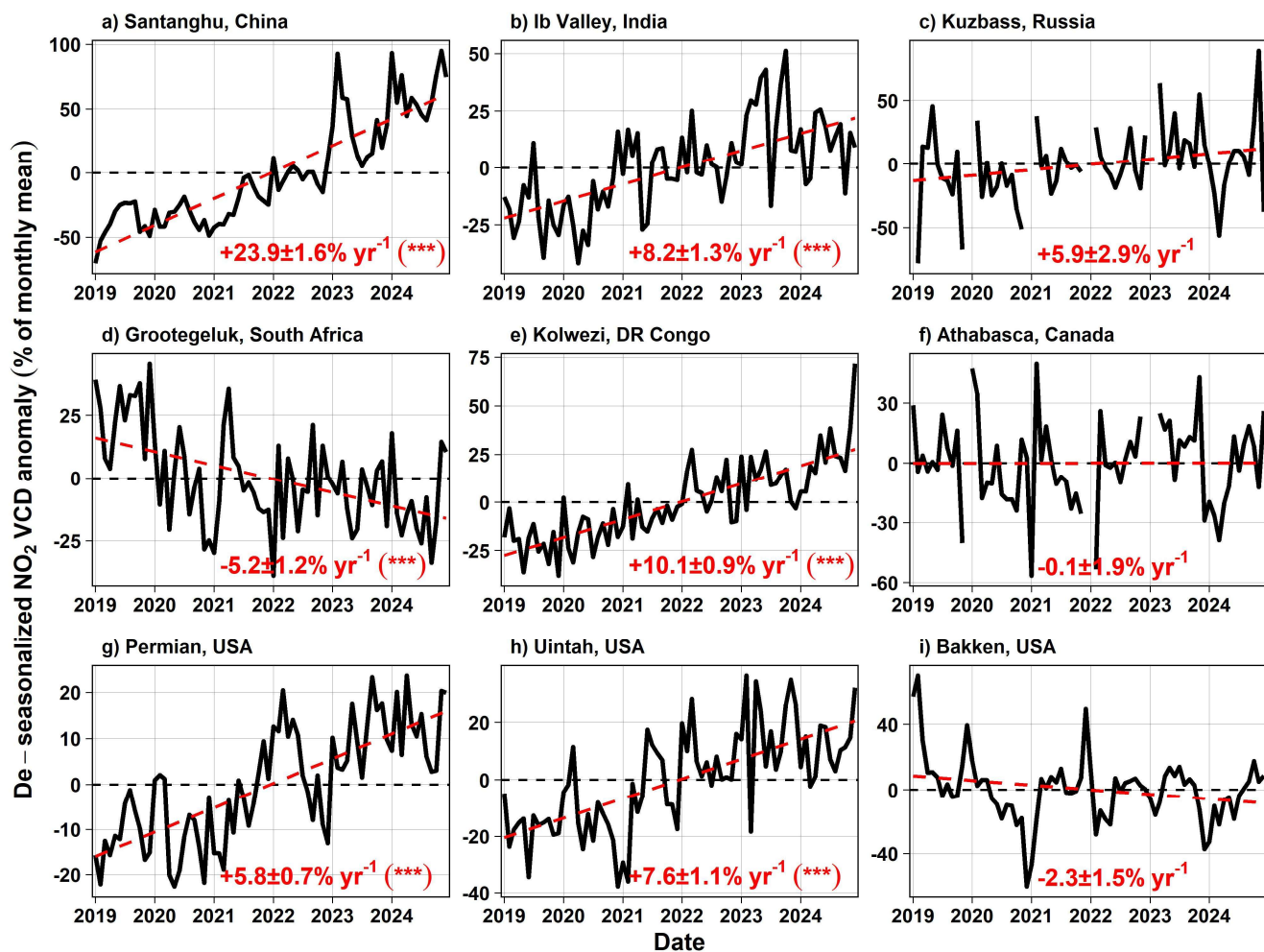
510 **6 TROPOMI NO₂ VCD changes in oil, gas and other mining regions**

511 NO₂ can be readily observed over oil, gas, and other mining regions due to emissions from drilling and extraction equipment,
512 processing plants, compressors, truck traffic, and routine or episodic flaring. In these settings, increases or decreases in NO₂
513 can signify shifts in production levels or changes in mining activity. Because NO₂ responds quickly to changes in combustion-
514 related activity, satellite retrievals serve as an effective proxy for monitoring relative operational intensity in major extraction
515 regions (Dix et al., 2022).

516 Known coal-dominated mining regions showed pronounced NO₂ VCD increases from 2019 to 2024 (Fig. 12). The sparsely-
517 populated Santanghu Basin (Fig. 12a), a region in eastern Xinjiang Province with a relatively nascent coal mining industry
518 (Zhang et al., 2018; Liu et al., 2018), represented the most substantial increase in VCD over China through 2024 (23.9±1.6%
519 yr⁻¹; p < 0.001). The recent expansion of mining operations is evident in visible satellite imagery (Fig. S20). The largest regional
520 increase in VCD anywhere in India from 2019 to 2024 (+2.1 × 10¹⁵ molecules cm⁻²) was observed in the Ib Valley in
521 northwestern Odisha state (Fig. 12b). The region contains multiple surface coal mines and coal-fired power plants (Varma et
522 al., 2015), with VCDs increasing at a rate of 8.2±1.3% yr⁻¹ (p < 0.001). NO₂ VCDs near numerous other coal mines and power
523 plants throughout India exhibited changes, but NO₂ VCD increases were more prevalent than decreases. In the Kuzbass Region
524 of Siberia, one of Russia's largest coal mining regions, 2024 annual mean VCDs were 2.4 × 10¹⁵ molecules cm⁻² higher than
525 in 2019, though no significant trend was observed (Fig. 12c). A previous study identified a correlation between space-based
526 NO₂ observations and regional coal production in the Kuzbass region (Labzovskii et al., 2022), providing relevant context for
527 the observed VCD changes. Increased VCDs were also observed over rare earth metal mines. In a mining region known as the
528 Copperbelt in the south of the Democratic Republic of the Congo (DRC), broad NO₂ VCD increases were observed, including
529 at a large surface copper and cobalt mine near the city of Kolwezi (Fig. 12e). VCDs at the Kolwezi mine increased at a rate of
530 10.1±0.9% yr⁻¹ (p < 0.001) from 2019 to 2024. Numerous surface mines exist in the region, with most observing increases in
531 NO_x emissions from mining operations in recent years (Martínez-Alonso et al., 2023).

532 Not all coal regions experienced increased VCDs. Northwest of Johannesburg, South Africa in Limpopo Province, NO₂ VCDs
533 near the Grootegeluk surface coal mine, together with two adjacent power plants (Faure et al., 2010; Shikwambana et al., 2020)
534 decreased at a rate of -5.2±1.2% yr⁻¹ (p < 0.001) from 2019 to 2024 (Fig. 12d). The region represented one of the largest NO₂
535 signatures in Africa in 2024, despite the decreasing trend for this period (Fig. 8a).

536 Oil and gas extraction areas in North America experienced diverse patterns. Annual mean NO₂ VCDs at the Athabasca oil
537 sands in Alberta, Canada were slightly lower in 2024 than in 2019, although the decreasing trend for the period was
538 insignificant (p > 0.05; Fig. 12f). The Bakken region in North Dakota, U.S. experienced a similarly insignificant decrease in
539 VCDs (Fig. 12i). Notable increases occurred in the Permian (Fig. 12g) and Uintah (Fig. 12h) Basins in the southwestern U.S.
540 experiencing increasing trends of 5.8±0.7% yr⁻¹ (p < 0.001) and 7.6±1.1% yr⁻¹ (p < 0.001), respectively.



542

543

544

545

546

Figure 12: Monthly time series of de-seasonalized NO₂ VCDs over selected oil, gas, and other mining regions. Black lines denote de-seasonalized VCDs, and dashed red lines represent trends characterized by ordinary least-squares regression for each site. Months with missing data lacked quality-assured TROPOMI observations. The % change yr⁻¹, standard error and statistical significance of each trend is reported each panel. Note the differing y-axis extents for each panel.

547 7 Conclusions

548 We present a global analysis of urban TROPOMI tropospheric NO₂ VCD trends from 2019 to 2024 using GHS-SMOD-defined
549 urban boundaries, encompassing more than 11,500 cities. Our results reveal ~~widespread decreases~~ statistically lower urban
550 population-weighted NO₂ VCDs in NO₂ across cities 2024 than in 2019 in Asia and Oceania (-17% on average), and Europe
551 (-17%), and North America (-5%), 13% with particularly strong reductions in cities including Seoul (-40%), 9.4±1.0% yr⁻¹; p
552 < 0.001), Guangzhou (-30%), 5.6±1.3% yr⁻¹; p < 0.001), and London, England (-34%), 5.4±1.3% yr⁻¹; p < 0.001). These
553 decreases generally reflect a combination of long-term emissions control policies and economic incentives, indicating
554 policy policies to tackle NO₂ pollution have broadly worked. COVID-19 induced reductions in activity often caused a
555 temporary NO₂ reduction but is unlikely to have caused much of the long-term changes between 2019 and 2024. Conversely,
556 urban NO₂ in Africa has gradually numerous African cities have increased over the same period, with Abidjan (+40%) 6.6±1.2%
557 yr⁻¹; p < 0.001), Cairo (+2.3±0.8% yr⁻¹; p = 0.006) and Addis Ababa (+35%) 2.4±1.1% yr⁻¹; p = 0.012) representing larger cities
558 that are leading the continent's upward trend. With Though numerous populous North American cities exhibited significant
559 VCD decreases, population-weighted urban levels for the exception of May-September in 2020 continent as a whole did not
560 show a significant change. Similarly, South America American cities exhibited little mean an insignificant VCD change from
561 2019 to 2024, with being Santiago (-19%) being a notable exception apart from May-September in 2020. Population-weighted
562 NO₂ VCDs increased-increases were most notable in countries in the Middle East and ~~much of~~ Africa, highlighting a potential
563 degradation in air quality in regions of the world that lack extensive ground-level monitoring.

564 Evaluating annual changes in TROPOMI NO₂ urban enhancements (VCD_{ENH})—the difference between mean urban and
565 background VCDs—against changes in EDGAR and CEDS NO_x emissions inventories, we show that highlight potential
566 discrepancies in inventory estimates in urban regions. In African, Asian and European cities, changes in VCD_{ENH} scales best
567 with-tend to exceed changes in both EDGAR and CEDS emissions, pointing to potential inventory overestimates in NO_x in
568 European and emissions. In North American cities, America, EDGAR agrees well with VCD_{ENH} (mean percent
569 differences difference of +5.7% and +0.23% relative to 2019 levels, respectively, and scale worse in other parts of the globe,
570 revealing potential discrepancies in emissions inventories. This mismatch is particularly evident in African (-7.7%) and Asian
571 (+8.3%) cities, and values), while CEDS NO_x emissions are 6.1% lower than VCD_{ENH}, relative to their respective 2019 values.
572 These mismatches may stem from rapidly evolving emission sources or limitations in the EDGAR and CEDS bottom-up
573 inventory methods. Similar discrepancies in emissions inventories in the Global South have been reported in previous studies
574 (Ahn et al., 2023), suggesting a systematic larger emissions underestimation uncertainties in regions where unmonitored
575 emissions activity may be significant.

576 In most regions, VCD trends from 2019 to 2024 were driven by changes during the colder months (November – March). This
577 was most pronounced in Asian cities, where mean cold season VCDs decreased by -1.2×10^{15} molecules cm⁻² (-18%) ~~on~~ from

578 2019 to 2024, compared with warm season VCD decreases of -0.5×10^{15} molecules cm^{-2} (-13%). Large changes in NO_2 were
579 not confined to urban regions alone. We identified localized increases near fossil fuel and other mining operations, including
580 in the Santanghu Basin in China ($+172\%$), $23.9 \pm 1.6\% \text{ yr}^{-1}$; $p < 0.001$), the Permian ($+19\%$) $5.8 \pm 0.7\% \text{ yr}^{-1}$; $p < 0.001$) and Uintah
581 ($+35\%$) $7.6 \pm 1.1\% \text{ yr}^{-1}$; $p < 0.001$) Basins in the U.S., and the Copperbelt region of the DRC ($+64\%$) $10.1 \pm 0.9\% \text{ yr}^{-1}$; $p < 0.001$),
582 signaling expanding industrial activity. In Khartoum and Kyiv, conflict and displacement drove sharp reductions in NO_2 ,
583 demonstrating the utility of satellite data in detecting societal disruptions.

584 Several limitations of this work should be noted. First, satellite NO_2 column densities may not always reflect surface-level NO_2
585 concentrations, particularly in regions with vertically elevated sources. In urban areas dominated by surface-based
586 transportation emissions, NO_2 VCDs are likely more representative of surface exposure. However, in areas with tall-stack
587 sources, such as power plants, NO_2 columns may be decoupled from near-surface levels- (Brett et al., 2025). Second, we
588 assume static city boundaries defined by the 2023 version of GHS-SMOD, with population estimates from 2020. This is likely
589 a reasonable approximation for urbanized regions in Europe and North America, where built-up area changes are slow, but
590 may introduce uncertainty in rapidly urbanizing regions of Africa and Asia over a six-year period. Future analyses could
591 incorporate time-varying urban boundaries to address this. Additionally, while many of the trends presented here reflect
592 changes in anthropogenic NO_x emissions, it is important to recognize that atmospheric chemistry also influences the observed
593 NO_2 variability. Seasonal differences in photochemical lifetimes (i.e., longest in winter), boundary layer mixing (i.e., more
594 vertical mixing in summer), chemical partitioning between NO and NO_2 (i.e., the fraction of NO_2 is largest in winter) and
595 meteorological variability can all modulate the magnitude and timing of observed trends. These processes likely contribute to
596 some of the regional and seasonal differences highlighted in this study.

597 Taken together, these results demonstrate the utility of high-resolution satellite instruments for characterizing both broad
598 regional trends and localized pollution changes, and linking with anthropogenically induced factors such as urban growth,
599 industrial expansion, policy interventions, and conflict. This highlights potential in using TROPOMI observations as an
600 accountability agent to determine how local changes in human activities affect local and global air pollution. As the TROPOMI
601 record lengthens and newer, geostationary satellites come online and begin to detect changes in atmospheric composition,
602 continued space-based monitoring will be essential for improving our understanding of atmospheric composition and chemistry
603 around the globe.

604 **Data Availability.**

605 The level 3 annual and monthly average TROPOMI NO_2 VCDs are available at 10.5067/ACADNS5UBWPQ and
606 <https://doi.org/10.5067/KKPPL39PEIGE>, respectively. The GHS-SMOD urban boundaries can be downloaded from
607 <https://human-settlement.emergency.copernicus.eu/download.php?ds=smod>. The EDGARv8 EDGARv8.1 NO_x emissions

608 can be downloaded from https://edgar.jrc.ec.europa.eu/dataset_ap81. The CEDS NO_x emissions can be downloaded from
609 <https://aims2.llnl.gov/>.

610 **Supplement.**

611 The supplement contains additional figures related to the study, including: S1 ~~All~~ Background NO₂ sensitivity in Beijing. S2
612 Background NO₂ sensitivity in Los Angeles. S3 Background NO₂ sensitivity in London. S4 Background NO₂ sensitivity in
613 Moscow. S5 Annual background NO₂ changes by continent. S6 Relative NO₂ VCD_{ENH} changes by continent. S7 Background
614 NO₂ for adjacent cities. S8 ~~GHS-SMOD urban clusters.~~ ~~S2 example.~~ S9 Data disaggregation example. ~~S3 Satellite view of~~
615 ~~surface mines.~~ S4 ~~Spatial plot of African NO₂.~~ S5-S10 Khartoum NO₂ time series. S6S11 NO₂ increases in three U.S. global
616 cities. S7 ~~Spatial plot of South American~~ S12 Annual mean NO₂. S8 in Tehran, Iran. S13 Annual mean NO₂ VCDs for
617 Bangladeshi cities. S9 ~~Annual mean NO₂ in Iran.~~ S10 ~~Annual mean VCDs in Chinese cities.~~ S11S14 Seasonal relative NO₂
618 changes by continent. S15 Annual mean NO₂ changes in the European Union. S12S16 Annual mean NO₂ changes in Russian
619 and Ukrainian cities. S13S17 Seasonal NO₂ changes by continent., without Russia. S18 NO₂ increases in three U.S. cities. S19
620 Satellite view of surface mines.

621 **Author Contribution.**

622 D.H. and D.G. contributed to the project design. D.G. processed and provided the annually- and monthly-averaged NO₂ vertical
623 column densities. All authors edited the manuscript.

624 **Competing Interests.**

625 The authors declare that they have no conflict of interest.

626 **Acknowledgements.**

627 This work was supported by National Aeronautics and Space Administration (NASA) Health and Air Quality Applied Sciences
628 Team (HAQAST) grant #80NSSC21K0511 and NASA Aura Atmospheric Composition Modeling and Analysis Program
629 (ACMAP) grant #80NSSC23K1002.

630

631 **References**

- 632 ~~Ahn, D. Y., Goldberg, D. L., Coombes, T., Kleiman, G., and Anenberg, S. C.: CO₂ emissions from C40 cities: citywide~~
633 ~~emission inventories and comparisons with global gridded emission datasets, *Environ. Res. Lett.*, 18, 034032,~~
634 ~~<https://doi.org/10.1088/1748-9326/ACBB91>, 2023.~~
- 635 ~~Anenberg, S. C., Mohegh, A., Goldberg, D. L., Kerr, G. H., Brauer, M., Burkart, K., Hystad, P., Larkin, A., Wozniak, S., and~~
636 ~~Lamsal, L.: Long-term trends in urban NO₂ concentrations and associated paediatric asthma incidence: estimates from~~
637 ~~global datasets, *Lancet Planet. Heal.*, 6, e49–e58, [https://doi.org/10.1016/S2542-5196\(21\)00255-](https://doi.org/10.1016/S2542-5196(21)00255-2/ATTACHMENT/7B9BB37F-5DEA-41D7-A9CC-9AFFA3989D6A/MMC1.PDF)~~
638 ~~[2/ATTACHMENT/7B9BB37F-5DEA-41D7-A9CC-9AFFA3989D6A/MMC1.PDF](https://doi.org/10.1016/S2542-5196(21)00255-2/ATTACHMENT/7B9BB37F-5DEA-41D7-A9CC-9AFFA3989D6A/MMC1.PDF), 2022.~~
- 639 ~~Bovensmann, H., Burrows, J. P., Buchwitz, M., Frerick, J., Noël, S., Rozanov, V. V., Chance, K. V., and Goede, A. P. H.:~~
640 ~~SCIAMACHY: Mission Objectives and Measurement Modes, *J. Atmos. Sci.*, 56, 127–150, [https://doi.org/10.1175/1520-](https://doi.org/10.1175/1520-0469(1999)056<0127:SMOAMM>2.0.CO;2)~~
641 ~~[0469\(1999\)056<0127:SMOAMM>2.0.CO;2](https://doi.org/10.1175/1520-0469(1999)056<0127:SMOAMM>2.0.CO;2), 1999.~~
- 642 ~~Burrows, J. P., Weber, M., Buchwitz, M., Rozanov, V., Ladstätter-Weissenmayer, A., Richter, A., Debeek, R., Hoogen, R.,~~
643 ~~Bramstedt, K., Eichmann, K. U., Eisinger, M., and Perner, D.: The Global Ozone Monitoring Experiment (GOME):~~
644 ~~Mission Concept and First Scientific Results, *J. Atmos. Sci.*, 56, 151–175, [https://doi.org/10.1175/1520-](https://doi.org/10.1175/1520-0469(1999)056<0151:TGOMEG>2.0.CO;2)~~
645 ~~[0469\(1999\)056<0151:TGOMEG>2.0.CO;2](https://doi.org/10.1175/1520-0469(1999)056<0151:TGOMEG>2.0.CO;2), 1999.~~
- 646 ~~Chen, X., Qi, L., Li, S., and Duan, X.: Long-term NO₂ exposure and mortality: A comprehensive meta-analysis, *Environ.*
647 ~~*Pollut.*, 341, 122971, <https://doi.org/10.1016/J.ENVPOL.2023.122971>, 2024.~~~~
- 648 ~~Cifuentes-Faura, J.: European Union policies and their role in combating climate change over the years, *Air Qual. Atmos.*
649 ~~*Heal.*, 15, 1333–1340, <https://doi.org/10.1007/S11869-022-01156-5/FIGURES/1>, 2022.~~~~
- 650 ~~Cooper, M. J., Martin, R. V., Hammer, M. S., Levelt, P. F., Veeffkind, P., Lamsal, L. N., Krotkov, N. A., Brook, J. R., and~~
651 ~~McLinden, C. A.: Global fine-scale changes in ambient NO₂ during COVID-19 lockdowns, *Nat.* 2022 6017893, 601,~~
652 ~~380–387, <https://doi.org/10.1038/s41586-021-04229-0>, 2022.~~
- 653 ~~Crippa, M., Guizzardi, D., Pagani, F., Schiavina, M., Melchiorri, M., Pisoni, E., Graziosi, F., Muntean, M., Maes, J., Dijkstra,~~
654 ~~L., Damme, M. Van, Clarisse, L., and Coheur, P.: Insights into the spatial distribution of global, national, and subnational~~
655 ~~greenhouse gas emissions in the Emissions Database for Global Atmospheric Research (EDGAR v8.0), *Earth Syst. Sci.*
656 ~~*Data*, 16, 2811–2830, <https://doi.org/10.5194/essd-16-2811-2024>, 2024.~~~~
- 657 ~~Cui, R. Y., Hultman, N., Cui, D., McJeon, H., Yu, S., Edwards, M. R., Sen, A., Song, K., Bowman, C., Clarke, L., Kang, J.,~~
658 ~~Lou, J., Yang, F., Yuan, J., Zhang, W., and Zhu, M.: A plant-by-plant strategy for high-ambition coal power phaseout in~~
659 ~~China, *Nat. Commun.* 2021 121, 12, 1–10, <https://doi.org/10.1038/s41467-021-21786-0>, 2021.~~

660 Dang, R., Jacob, D. J., Shah, V., Eastham, S. D., Fritz, T. M., Mickley, L. J., Liu, T., Wang, Y., and Wang, J.: Background
661 nitrogen dioxide (NO₂) over the United States and its implications for satellite observations and trends: effects of nitrate
662 photolysis, aircraft, and open fires, *Atmos. Chem. Phys.*, *23*, 6271–6284, <https://doi.org/10.5194/ACP-23-6271-2023>,
663 2023.

664 Dix, B., de Bruin, J., Roosenbrand, E., Vlemmix, T., Francoeur, C., Gorehov-Negron, A., McDonald, B., Zhizhin, M., Elvidge,
665 C., Veeffkind, P., Levelt, P., and de Gouw, J.: Nitrogen Oxide Emissions from U.S. Oil and Gas Production: Recent Trends
666 and Source Attribution, *Geophys. Res. Lett.*, *47*, e2019GL085866, <https://doi.org/10.1029/2019GL085866>, 2020.

667 Duncan, B. N., Lamsal, L. N., Thompson, A. M., Yoshida, Y., Lu, Z., Streets, D. G., Hurwitz, M. M., and Pickering, K. E.: A
668 space-based, high-resolution view of notable changes in urban NO_x pollution around the world (2005–2014), *J. Geophys.*
669 *Res.*, *121*, 976–996, <https://doi.org/10.1002/2015JD024121>, 2016.

670 Faure, K., Willis, J. P., and Dreyer, J. C.: The grootegeluk formation in the Waterberg Coalfield, South Africa: facies,
671 palaeoenvironment and thermal history—evidence from organic and elastic matter, *Int. J. Coal Geol.*, *29*, 147–186,
672 [https://doi.org/10.1016/0166-5162\(95\)00029-1](https://doi.org/10.1016/0166-5162(95)00029-1), 1996.

673 Fioletov, V., Melinden, C. A., Griffin, D., Krotkov, N., Liu, F., and Eskes, H.: Quantifying urban, industrial, and background
674 changes in NO₂ during the COVID-19 lockdown period based on TROPOMI satellite observations, *Atmos. Chem. Phys.*,
675 *22*, 4201–4236, <https://doi.org/10.5194/acp-22-4201-2022>, 2022.

676 Fioletov, V., Melinden, C. A., Griffin, D., Zhao, X., and Eskes, H.: Global seasonal urban, industrial, and background NO₂
677 estimated from TROPOMI satellite observations, *Atmos. Chem. Phys.*, *25*, 575–596, [https://doi.org/10.5194/acp-25-575-](https://doi.org/10.5194/acp-25-575-2025)
678 2025, 2025.

679 Fisher, B. L., Lamsal, L. N., Fasnacht, Z., Oman, L. D., Joiner, J., Krotkov, N. A., Choi, S., Qin, W., and Yang, E. S.: Revised
680 estimates of NO₂ reductions during the COVID-19 lockdowns using updated TROPOMI NO₂ retrievals and model
681 simulations, *Atmos. Environ.*, *326*, 120459, <https://doi.org/10.1016/J.ATMOSENV.2024.120459>, 2024.

682 Fishman, J., Iraci, L. T., Al-Saadi, J., Chance, K., Chavez, F., Chin, M., Coble, P., Davis, C., DiGiacomo, P. M., Edwards, D.,
683 Eldering, A., Goes, J., Herman, J., Hu, C., Jacob, D. J., Jordan, C., Kawa, S. R., Key, R., Liu, X., Lohrenz, S., Mannino,
684 A., Natraj, V., Neil, D., Neu, J., Newchurch, M., Pickering, K., Salisbury, J., Sosik, H., Subramaniam, A., Tzortziou, M.,
685 Wang, J., and Wang, M.: The United States’ Next Generation of Atmospheric Composition and Coastal Ecosystem
686 Measurements: NASA’s Geostationary Coastal and Air Pollution Events (GEO-CAPE) Mission, *Bull. Am. Meteorol.*
687 *Soc.*, *93*, 1547–1566, <https://doi.org/10.1175/BAMS-D-11-00201.1>, 2012.

688 De Foy, B., Lu, Z., and Streets, D. G.: Satellite NO₂ retrievals suggest China has exceeded its NO_x reduction goals from the
689 twelfth Five-Year Plan, *Sci. Reports* 2016-61, *6*, 1–9, <https://doi.org/10.1038/srep35912>, 2016.

690 Geddes, J. A., Martin, R. V., Boys, B. L., and van Donkelaar, A.: Long term trends worldwide in ambient NO₂ concentrations
691 inferred from satellite observations, *Environ. Health Perspect.*, 124, 281–289,
692 https://doi.org/10.1289/EHP.1409567/SUPPL_FILE/EHP.1409567.S001.ACCO.PDF, 2016.

693 Van Geffen, J., Eskes, H., Compernelle, S., Pinardi, G., Verhoelst, T., Lambert, J. C., Sneep, M., Linden, M. Ter, Ludewig,
694 A., Folkert-Boersma, K., and Pepijn Veeffkind, J.: Sentinel 5P TROPOMI NO₂ retrieval: impact of version v2.2
695 improvements and comparisons with OMI and ground based data, *Atmos. Meas. Tech.*, 15, 2037–2060,
696 <https://doi.org/10.5194/amt-15-2037-2022>, 2022.

697 Goldberg, D.: HAQAST Sentinel 5P TROPOMI Nitrogen Dioxide (NO₂) GLOBAL Monthly Level 3 0.1 x 0.1 Degree
698 Gridded Data Version 2.4 (HAQ_TROPOMI_NO2_GLOBAL_M_L3) at GES DISC,
699 <https://doi.org/10.5067/KKPPL39PEIGE>, 15 March 2024.

700 Goldberg, D. L., Anenberg, S. C., Kerr, G. H., Mohegh, A., Lu, Z., and Streets, D. G.: TROPOMI NO₂ in the United States:
701 A Detailed Look at the Annual Averages, Weekly Cycles, Effects of Temperature, and Correlation With Surface NO₂
702 Concentrations, *Earth's Futur.*, 9, <https://doi.org/10.1029/2020EF001665>, 2021.

703 Goldberg, D.L.: HAQAST Sentinel 5P TROPOMI Nitrogen Dioxide (NO₂) GLOBAL Monthly Level 3 0.1 x 0.1 Degree
704 Gridded Data Version 2.4 (HAQ_TROPOMI_NO2_GLOBAL_M_L3) at GES DISC, Goddard Earth Sciences Data and
705 Information Services Center (GES DISC), <https://doi.org/10.5067/KKPPL39PEIGE>, 2024.

706 Goldberg, D. L., Tao, M., Kerr, G. H., Ma, S., Tong, D. Q., Fiore, A. M., Dickens, A. F., Adelman, Z. E., and Anenberg, S.
707 C.: Evaluating the spatial patterns of U.S. urban NO_x emissions using TROPOMI NO₂, *Remote Sens. Environ.*, 300,
708 <https://doi.org/10.1016/j.rse.2023.113917>, 2024.

709 de Gouw, J. A., Veeffkind, J. P., Roosenbrand, E., Dix, B., Lin, J. C., Landgraf, J., and Levelt, P. F.: Daily Satellite Observations
710 of Methane from Oil and Gas Production Regions in the United States, *Sci. Rep.*, 10, 1–10,
711 [https://doi.org/10.1038/S41598-020-57678-](https://doi.org/10.1038/S41598-020-57678-4)
712 [4](https://doi.org/10.1038/S41598-020-57678-4);TECHMETA=134;SUBJMETA=106,169,172,35,704,824;KWRD=ATMOSPHERIC+CHEMISTRY, 2020.

713 Guo, Z., Abushama, H., Siddig, K., Kirui, O. K., Abay, K., and You, L.: Monitoring Indicators of Economic Activities in
714 Sudan Amidst Ongoing Conflict Using Satellite Data, *Def. Peace Econ.*,
715 <https://doi.org/10.1080/10242694.2023.2290474>;PAGE:STRING:ARTICLE/CHAPTER, 2023.

716 Hajmohammadi, H. and Heydecker, B.: Evaluation of air quality effects of the London ultra-low emission zone by state-space
717 modelling, *Atmos. Pollut. Res.*, 13, 1015–14, <https://doi.org/10.1016/J.APR.2022.101514>, 2022.

718 Harake, W., Jamali, I., and Abou Hamde, N.: Lebanon Economic Monitor : Lebanon Sinking (to the Top 3), Washington, D.C.,
719 <https://doi.org/http://documents.worldbank.org/curated/en/394741622469174252>, 2021.

720 Herman, J., Cede, A., Spinei, E., Mount, G., Tzortziou, M., and Abuhassan, N.: NO₂ column amounts from ground-based
721 Pandora and MFDOAS spectrometers using the direct sun DOAS technique: Intercomparisons and application to OMI
722 validation, *J. Geophys. Res. Atmos.*, 114, <https://doi.org/10.1029/2009JD011848>, 2009.

723 Hersbach, H., Bell, B., Berrisford, P., Hirahara, S., Horányi, A., Muñoz Sabater, J., Nicolas, J., Peubey, C., Radu, R., Schepers,
724 D., Simmons, A., Soci, C., Abdalla, S., Abellan, X., Balsamo, G., Bechtold, P., Biavati, G., Bidlot, J., Bonavita, M., De
725 Chiara, G., Dahlgren, P., Dee, D., Diamantakis, M., Dragani, R., Flemming, J., Forbes, R., Fuentes, M., Geer, A.,
726 Haimberger, L., Healy, S., Hogan, R. J., Hólm, E., Janisková, M., Keeley, S., Laloyaux, P., Lopez, P., Lupu, C., Radnoti,
727 G., de Rosnay, P., Rozum, I., Vamborg, F., Villaume, S., and Thépaut, J. N.: The ERA5 global reanalysis, *Q. J. R.
728 Meteorol. Soc.*, 146, 1999–2049, <https://doi.org/10.1002/QJ.3803>, 2020.

729 Ho, C. H., Heo, J. W., Chang, M., Choi, W., Kim, J., Kim, S. W., and Oh, H. R.: Regulatory measures significantly reduced
730 air pollutant concentrations in Seoul, Korea, *Atmos. Pollut. Res.*, 12, 101098,
731 <https://doi.org/10.1016/J.APR.2021.101098>, 2021.

732 Huber, D. E., Kort, E. A., and Steiner, A. L.: Soil Moisture, Soil NO_x and Regional Air Quality in the Agricultural Central
733 United States, *J. Geophys. Res. Atmos.*, 129, e2024JD041015, <https://doi.org/10.1029/2024JD041015>, 2024.

734 Jiang, Z., McDonald, B. C., Worden, H., Worden, J. R., Miyazaki, K., Qu, Z., Henze, D. K., Jones, D. B. A., Arellano, A. F.,
735 Fischer, E. V., Zhu, L., and Folkert Boersma, K.: Unexpected slowdown of US pollutant emission reduction in the past
736 decade, *Proc. Natl. Acad. Sci. U. S. A.*, 115, 5099–5104, <https://doi.org/10.1073/PNAS.1801191115/>
737 /DCSUPPLEMENTAL, 2018.

738 Jiang, Z., Zhu, R., Miyazaki, K., McDonald, B. C., Klimont, Z., Zheng, B., Boersma, K. F., Zhang, Q., Worden, H., Worden,
739 J. R., Henze, D. K., Jones, D. B. A., Denier van der Gon, H. A. C., and Eskes, H.: Decadal Variabilities in Tropospheric
740 Nitrogen Oxides Over United States, Europe, and China, *J. Geophys. Res. Atmos.*, 127, e2021JD035872,
741 <https://doi.org/10.1029/2021JD035872>, 2022.

742 Jin, X., Zhu, Q., Cohen, R. C., and Xiaomeng, J.: Direct estimates of biomass burning NO_x emissions and lifetimes using
743 daily observations from TROPOMI, *Atmos. Chem. Phys.*, 21, 15569–15587, <https://doi.org/10.5194/acp-21-15569-2021>,
744 2021.

745 Kim, E. J., Holloway, T., Kokandakar, A., Harkey, M., Elkins, S., Goldberg, D. L., and Heck, C.: A Comparison of Regression
746 Methods for Inferring Near Surface NO₂ With Satellite Data, *J. Geophys. Res. Atmos.*, 129, e2024JD040906,
747 <https://doi.org/10.1029/2024JD040906>, 2024.

748 Krotkov, N. A., Melinden, C. A., Li, C., Lamsal, L. N., Celarier, E. A., Marchenko, S. V., Swartz, W. H., Buesela, E. J., Joiner,
749 J., Duncan, B. N., Folkert Boersma, K., Pepijn Veefkind, J., Levelt, P. F., Fioletov, V. E., Dickerson, R. R., He, H., Lu,

750 Z., and Streets, D. G.: Aura OMI observations of regional SO₂ and NO₂ pollution changes from 2005 to 2015, *Atmos.*
751 *Chem. Phys.*, 16, 4605–4629, <https://doi.org/10.5194/acp-16-4605-2016>, 2016.

752 Labzovskii, L. D., Belikov, D. A., and Damiani, A.: Spaceborne NO₂ observations are sensitive to coal mining and processing
753 in the largest coal basin of Russia, *Sci. Rep.*, 12, 1–11, [https://doi.org/10.1038/S41598-022-16850-](https://doi.org/10.1038/S41598-022-16850-8)
754 [8](https://doi.org/10.1038/S41598-022-16850-8);SUBJMETA=106,172,35,4081,704;KWRD=ATMOSPHERIC+SCIENCE,ENVIRONMENTAL+IMPACT,ENVIRO-
755 NMENTAL+SCIENCES, 2022.

756 Lamsal, L. N., Duncan, B. N., Yoshida, Y., Krotkov, N. A., Pickering, K. E., Streets, D. G., and Lu, Z.: U.S. NO₂ trends
757 (2005–2013): EPA Air Quality System (AQS) data versus improved observations from the Ozone Monitoring Instrument
758 (OMI), *Atmos. Environ.*, 110, 130–143, <https://doi.org/10.1016/J.ATMOSENV.2015.03.055>, 2015.

759 Laughner, J. L. and Cohen, R. C.: Direct observation of changing NO_x lifetime in North American cities, *Science* (80-.), 366,
760 723–727, <https://doi.org/10.1126/science.aax6832>, 2019.

761 Levelt, P. F., Van Den Oord, G. H. J., Dobber, M. R., Mälkki, A., Visser, H., De Vries, J., Stammes, P., Lundell, J. O. V., and
762 Saari, H.: The ozone monitoring instrument, *IEEE Trans. Geosci. Remote Sens.*, 44, 1093–1100,
763 <https://doi.org/10.1109/TGRS.2006.872333>, 2006.

764 Li, H., Zheng, B., Lei, Y., Hauglustaine, D., Chen, C., Lin, X., Zhang, Y., Zhang, Q., and He, K.: Trends and drivers of
765 anthropogenic NO_x emissions in China since 2020, *Environ. Sci. Ecotechnology*, 21, 100425,
766 <https://doi.org/10.1016/J.ESE.2024.100425>, 2024.

767 Liu, B., Fu, X., Bechtel, A., Gross, D., Sachsenhofer, R. F., and Li, X.: Middle Permian environmental changes and shale oil
768 potential evidenced by high resolution organic petrology, geochemistry and mineral composition of the sediments in the
769 Santanghu Basin, Northwest China, *Int. J. Coal Geol.*, 185, 119–137, <https://doi.org/10.1016/J.COAL.2017.11.015>, 2018.

770 Liu, F., Zhang, Q., Van Der A, R. J., Zheng, B., Tong, D., Yan, L., Zheng, Y., and He, K.: Recent reduction in NO_x emissions
771 over China: synthesis of satellite observations and emission inventories, *Environ. Res. Lett.*, 11, 114002,
772 <https://doi.org/10.1088/1748-9326/11/11/114002>, 2016.

773 Lonsdale, C. R. and Sun, K.: Nitrogen oxides emissions from selected cities in North America, Europe, and East Asia observed
774 by the TROPospheric Monitoring Instrument (TROPOMI) before and after the COVID-19 pandemic, *Atmos. Chem.*
775 *Phys.*, 23, 8727–8748, <https://doi.org/10.5194/acp-23-8727-2023>, 2023.

776 Ma, Q., Wang, J., Xiong, M., and Zhu, L.: Air Quality Index (AQI) Did Not Improve during the COVID-19 Lockdown in
777 Shanghai, China, in 2022, Based on Ground and TROPOMI Observations, *Remote Sens.*, 15, 1295,
778 <https://doi.org/10.3390/RS15051295/S1>, 2023.

779 Martínez Alonso, S., Veeffkind, J. P., Dix, B., Gaubert, B., Theys, N., Granier, C., Soulié, A., Darras, S., Eskes, H., Tang, W.,
780 Worden, H., de Gouw, J., and Levelt, P. F.: S-5P/TROPOMI Derived NO_x Emissions From Copper/Cobalt Mining and
781 Other Industrial Activities in the Copperbelt (Democratic Republic of Congo and Zambia), *Geophys. Res. Lett.*, *50*,
782 e2023GL104109, <https://doi.org/10.1029/2023GL104109>, 2023.

783 Matthias, V., Quante, M., Arndt, J. A., Badeke, R., Fink, L., Petrik, R., Feldner, J., Schwarzkopf, D., Link, E. M., Ramacher,
784 M. O. P., and Wedemann, R.: The role of emission reductions and the meteorological situation for air quality
785 improvements during the COVID-19 lockdown period in central Europe, *Atmos. Chem. Phys.*, *21*, 13931–13971,
786 <https://doi.org/10.5194/ACP-21-13931-2021>, 2021.

787 Miyazaki, K., Eskes, H., Sudo, K., Folkert Boersma, K., Bowman, K., and Kanaya, Y.: Decadal changes in global surface NO_x
788 emissions from multi-constituent satellite data assimilation, *Atmos. Chem. Phys.*, *17*, 807–837,
789 <https://doi.org/10.5194/ACP-17-807-2017>, 2017.

790 Panda, M. R., Tyagi, A., Dhanya, C. T., Verma, A., and Swain, A.: Vulnerability assessment of thermal power plants in India
791 under water stress conditions, *Energy*, *276*, 127553, <https://doi.org/10.1016/J.ENERGY.2023.127553>, 2023.

792 Richter, A., Burrows, J. P., Nüß, H., Granier, C., and Niemeier, U.: Increase in tropospheric nitrogen dioxide over China
793 observed from space, *Nature*, *437*, 129–132, <https://doi.org/10.1038/nature04092>, 2005.

794 Rokieki, T., Bórawski, P., and Szeberényi, A.: The Impact of the 2020–2022 Crises on EU Countries' Independence from
795 Energy Imports, Particularly from Russia, *Energies* *2023*, Vol. 16, Page 6629, 16, 6629,
796 <https://doi.org/10.3390/EN16186629>, 2023.

797 Schiavina M., Melchiorri M. & Pesaresi M.: GHS SMOD R2023A—GHS settlement layers, application of the Degree of
798 Urbanisation methodology (stage I) to GHS POP R2023A and GHS BUILT S R2023A, multitemporal (1975–2030).
799 European Commission, Joint Research Centre (JRC). [https://doi.org/10.2905/A0DF7A6F-49DE-46EA-9BDE-
800 563437A6E2BA](https://doi.org/10.2905/A0DF7A6F-49DE-46EA-9BDE-563437A6E2BA), 2023.

801 Schumann, U. and Huntrieser, H.: The global lightning induced nitrogen oxides source, *Atmos. Chem. Phys.*, *7*, 3823–3907,
802 2007.

803 SEDAC: The Gridded Population of the World (GPW), <https://sedac.ciesin.columbia.edu/data/collection/gpw-v4> (last access:
804 25 June 2024), 2017.

805 Seo, S., Kim, S. W., Kim, K. M., Lamsal, L. N., and Jin, H.: Reductions in NO₂ concentrations in Seoul, South Korea detected
806 from space and ground-based monitors prior to and during the COVID-19 pandemic, *Environ. Res. Commun.*, *3*, 051005,
807 <https://doi.org/10.1088/2515-7620/ABED92>, 2021.

808 Shi, Q., Zheng, B., Zheng, Y., Tong, D., Liu, Y., Ma, H., Hong, C., Geng, G., Guan, D., He, K., and Zhang, Q.: Co-benefits of
809 CO₂ emission reduction from China's clean air actions between 2013–2020, *Nat. Commun.* 2022 131, 13, 1–8,
810 <https://doi.org/10.1038/s41467-022-32656-8>, 2022.

811 Shikwambana, L., Mhangara, P., and Mbatha, N.: Trend analysis and first time observations of sulphur dioxide and nitrogen
812 dioxide in South Africa using TROPOMI/Sentinel 5 P data, *Int. J. Appl. Earth Obs. Geoinf.*, 91, 102130,
813 <https://doi.org/10.1016/J.JAG.2020.102130>, 2020.

814 Song, W., Liu, X. Y., Hu, C. C., Chen, G. Y., Liu, X. J., Walters, W. W., Michalski, G., and Liu, C. Q.: Important contributions
815 of non fossil fuel nitrogen oxides emissions, *Nat. Commun.* 2021 121, 12, 1–7, [https://doi.org/10.1038/s41467-020-](https://doi.org/10.1038/s41467-020-20356-0)
816 [20356-0](https://doi.org/10.1038/s41467-020-20356-0), 2021.

817 Stavrakou, T., Müller, J. F., Boersma, K. F., De Smedt, I., and van der A, R. J.: Assessing the distribution and growth rates of
818 NO_x emission sources by inverting a 10 year record of NO₂ satellite columns, *Geophys. Res. Lett.*, 35,
819 <https://doi.org/10.1029/2008GL033521>, 2008.

820 VanDerA, R. J., Eskes, H. J., Boersma, K. F., van Noije, T. P. C., Van Roozendaal, M., De Smedt, I., Peters, D. H. M. U., and
821 Meijer, E. W.: Trends, seasonal variability and dominant NO_x source derived from a ten year record of NO₂ measured
822 from space, *J. Geophys. Res. Atmos.*, 113, 1–12, <https://doi.org/10.1029/2007JD009021>, 2008.

823 Varma, A. K., Biswal, S., Hazra, B., Mendhe, V. A., Misra, S., Samad, S. K., Singh, B. D., Dayal, A. M., and Mani, D.:
824 Petrographic characteristics and methane sorption dynamics of coal and shaly coal samples from Ib Valley Basin, Odisha,
825 India, *Int. J. Coal Geol.*, 141–142, 51–62, <https://doi.org/10.1016/J.COAL.2015.03.005>, 2015.

826 Veefkind, J. P., Aben, I., McMullan, K., Förster, H., de Vries, J., Otter, G., Claas, J., Eskes, H. J., de Haan, J. F., Kleipool, Q.,
827 van Weele, M., Hasekamp, O., Hoogeveen, R., Landgraf, J., Snel, R., Tol, P., Ingmann, P., Voors, R., Kruizinga, B., Vink,
828 R., Visser, H., and Levelt, P. F.: TROPOMI on the ESA Sentinel 5 Precursor: A GMES mission for global observations
829 of the atmospheric composition for climate, air quality and ozone layer applications, *Remote Sens. Environ.*, 120, 70–83,
830 <https://doi.org/10.1016/J.RSE.2011.09.027>, 2012.

831 Zhang, Y., Tian, J., Feng, S., Yang, F., and Lu, X.: The occurrence modes and geologic origins of arsenic in coal from
832 Santanghu Coalfield, Xinjiang, *J. Geochemical Explor.*, 186, 225–234, <https://doi.org/10.1016/J.GEXPLO.2017.12.006>,
833 2018.

834 Zhao, X., Li, X. X., Xin, R., Zhang, Y., and Liu, C. H.: Impact of Lockdowns on Air Pollution: Case Studies of Two Periods
835 in 2022 in Guangzhou, China, *Atmos.* 2024, Vol. 15, Page 1144, 15, 1144, <https://doi.org/10.3390/ATMOS15091144>,
836 2024.

837 [Zheng, B., Zhang, Q., Geng, G., Chen, C., Shi, Q., Cui, M., Lei, Y., and He, K.: Changes in China's anthropogenic emissions](#)
838 [and air quality during the COVID-19 pandemic in 2020, *Earth Syst. Sci. Data*, 13, 2895–2907, \[https://doi.org/10.5194/ESSD-\]\(https://doi.org/10.5194/ESSD-13-2895-2021\)](#)
839 [13-2895-2021, 2021.](#)

840 [Ahn, D. Y., Goldberg, D. L., Coombes, T., Kleiman, G., and Anenberg, S. C.: CO2 emissions from C40 cities: citywide](#)
841 [emission inventories and comparisons with global gridded emission datasets, *Environmental Research Letters*, 18, 034032,](#)
842 [https://doi.org/10.1088/1748-9326/ACBB91, 2023.](#)

843 [Anenberg, S. C., Mohegh, A., Goldberg, D. L., Kerr, G. H., Brauer, M., Burkart, K., Hystad, P., Larkin, A., Wozniak, S., and](#)
844 [Lamsal, L.: Long-term trends in urban NO2 concentrations and associated paediatric asthma incidence: estimates from](#)
845 [global datasets, *Lancet Planet Health*, 6, e49–e58, \[https://doi.org/10.1016/S2542-5196\\(21\\)00255-\]\(https://doi.org/10.1016/S2542-5196\(21\)00255-2/ATTACHMENT/7B9BB37F-5DEA-41D7-A9CC-9AFFA3989D6A/MMC1.PDF\)](#)
846 [2/ATTACHMENT/7B9BB37F-5DEA-41D7-A9CC-9AFFA3989D6A/MMC1.PDF, 2022.](#)

847 [Bovensmann, H., Burrows, J. P., Buchwitz, M., Frerick, J., Noël, S., Rozanov, V. V., Chance, K. V., and Goede, A. P. H.:](#)
848 [SCIAMACHY: Mission Objectives and Measurement Modes, *J Atmos Sci*, 56, 127–150, \[https://doi.org/10.1175/1520-\]\(https://doi.org/10.1175/1520-0469\(1999\)056<0127:SMOAMM>2.0.CO;2\)](#)
849 [0469\(1999\)056<0127:SMOAMM>2.0.CO;2, 1999.](#)

850 [Brett, N., Arnold, S. R., Law, K. S., Raut, J.-C., Onishi, T., Barret, B., Dieudonné, E., Cesler-Maloney, M., Simpson, W.,](#)
851 [Bekki, S., Savarino, J., Albertin, S., Gilliam, R., Fahey, K., Pouliot, G., Huff, D., and D'Anna, B.: Estimating Power Plant](#)
852 [Contributions to Surface Pollution in a Wintertime Arctic Environment, *ACS ES&T Air*, 2, 943–956,](#)
853 [https://doi.org/10.1021/ACSESTAIR.5C00030, 2025.](#)

854 [Burrows, J. P., Weber, M., Buchwitz, M., Rozanov, V., Ladstätter-Weissenmayer, A., Richter, A., Debeek, R., Hoogen, R.,](#)
855 [Bramstedt, K., Eichmann, K. U., Eisinger, M., and Perner, D.: The Global Ozone Monitoring Experiment \(GOME\):](#)
856 [Mission Concept and First Scientific Results, *J Atmos Sci*, 56, 151–175, \[https://doi.org/10.1175/1520-\]\(https://doi.org/10.1175/1520-0469\(1999\)056<0151:TGOMEG>2.0.CO;2\)](#)
857 [0469\(1999\)056<0151:TGOMEG>2.0.CO;2, 1999.](#)

858 [Castellanos, P., Boersma, K. F., and Van Der Werf, G. R.: Satellite observations indicate substantial spatiotemporal variability](#)
859 [in biomass burning NOx emission factors for South America, *Atmos Chem Phys*, 14, 3929–3943,](#)
860 [https://doi.org/10.5194/ACP-14-3929-2014, 2014.](#)

861 [Chen, X., Qi, L., Li, S., and Duan, X.: Long-term NO2 exposure and mortality: A comprehensive meta-analysis, *Environmental*](#)
862 [Pollution, 341, 122971, <https://doi.org/10.1016/J.ENVPOL.2023.122971>, 2024.](#)

863 [Cifuentes-Faura, J.: European Union policies and their role in combating climate change over the years, *Air Qual Atmos*](#)
864 [Health, 15, 1333–1340, <https://doi.org/10.1007/S11869-022-01156-5/FIGURES/1>, 2022.](#)

865 [Cooper, M. J., Martin, R. V., Hammer, M. S., Levelt, P. F., Veeffkind, P., Lamsal, L. N., Krotkov, N. A., Brook, J. R., and](#)
866 [McLinden, C. A.: Global fine-scale changes in ambient NO2 during COVID-19 lockdowns, *Nature* 2022 601:7893, 601,](#)
867 [380–387, <https://doi.org/10.1038/s41586-021-04229-0>, 2022.](#)

868 [Crippa, M., Guizzardi, D., Muntean, M., Schaaf, E., Dentener, F., Van Aardenne, J. A., Monni, S., Doering, U., Olivier, J. G.](#)
869 [J., Pagliari, V., and Janssens-Maenhout, G.: Gridded emissions of air pollutants for the period 1970-2012 within EDGAR](#)
870 [v4.3.2, Earth Syst Sci Data, 10, 1987–2013, <https://doi.org/10.5194/ESSD-10-1987-2018>, 2018.](#)

871 [Crippa, M., Guizzardi, D., Pagani, F., Schiavina, M., Melchiorri, M., Pisoni, E., Graziosi, F., Muntean, M., Maes, J., Dijkstra,](#)
872 [L., Damme, M. Van, Clarisse, L., and Coheur, P.: Insights into the spatial distribution of global, national, and subnational](#)
873 [greenhouse gas emissions in the Emissions Database for Global Atmospheric Research \(EDGAR v8.0\), Earth Syst. Sci.](#)
874 [Data, 16, 2811–2830, <https://doi.org/10.5194/essd-16-2811-2024>, 2024.](#)

875 [Cui, R. Y., Hultman, N., Cui, D., McJeon, H., Yu, S., Edwards, M. R., Sen, A., Song, K., Bowman, C., Clarke, L., Kang, J.,](#)
876 [Lou, J., Yang, F., Yuan, J., Zhang, W., and Zhu, M.: A plant-by-plant strategy for high-ambition coal power phaseout in](#)
877 [China, Nature Communications 2021 12:1, 12, 1–10, <https://doi.org/10.1038/s41467-021-21786-0>, 2021.](#)

878 [Dang, R., Jacob, D. J., Shah, V., Eastham, S. D., Fritz, T. M., Mickley, L. J., Liu, T., Wang, Y., and Wang, J.: Background](#)
879 [nitrogen dioxide \(NO₂\) over the United States and its implications for satellite observations and trends: effects of nitrate](#)
880 [photolysis, aircraft, and open fires, Atmos Chem Phys, 23, 6271–6284, <https://doi.org/10.5194/ACP-23-6271-2023>, 2023.](#)

881 [Dix, B., de Bruin, J., Roosenbrand, E., Vlemmix, T., Francoeur, C., Gorchov-Negron, A., McDonald, B., Zhizhin, M., Elvidge,](#)
882 [C., Veefkind, P., Levelt, P., and de Gouw, J.: Nitrogen Oxide Emissions from U.S. Oil and Gas Production: Recent Trends](#)
883 [and Source Attribution, Geophys Res Lett, 47, e2019GL085866, <https://doi.org/10.1029/2019GL085866>, 2020.](#)

884 [Dix, B., Francoeur, C., Li, M., Serrano-Calvo, R., Levelt, P. F., Veefkind, J. P., McDonald, B. C., and de Gouw, J.: Quantifying](#)
885 [NO_x Emissions from U.S. Oil and Gas Production Regions Using TROPOMI NO₂, ACS Earth Space Chem, 6, 403–414,](#)
886 [\[https://doi.org/10.1021/ACSEARTHSPACECHEM.1C00387/ASSET/IMAGES/LARGE/SP1C00387_0008.JPEG\]\(https://doi.org/10.1021/ACSEARTHSPACECHEM.1C00387/ASSET/IMAGES/LARGE/SP1C00387_0008.JPEG\),](#)
887 [2022.](#)

888 [Duncan, B. N., Lamsal, L. N., Thompson, A. M., Yoshida, Y., Lu, Z., Streets, D. G., Hurwitz, M. M., and Pickering, K. E.: A](#)
889 [space-based, high-resolution view of notable changes in urban NO_x pollution around the world \(2005–2014\), J Geophys](#)
890 [Res, 121, 976–996, <https://doi.org/10.1002/2015JD024121>, 2016.](#)

891 [Faure, K., Willis, J. P., and Dreyer, J. C.: The grootegeeluk formation in the Waterberg Coalfield, South Africa: facies,](#)
892 [palaeoenvironment and thermal history — evidence from organic and clastic matter, Int J Coal Geol, 29, 147–186,](#)
893 [\[https://doi.org/10.1016/0166-5162\\(95\\)00029-1\]\(https://doi.org/10.1016/0166-5162\(95\)00029-1\), 1996.](#)

894 [Fioletov, V., McLinden, C. A., Griffin, D., Krotkov, N., Liu, F., and Eskes, H.: Quantifying urban, industrial, and background](#)
895 [changes in NO₂ during the COVID-19 lockdown period based on TROPOMI satellite observations, Atmos. Chem. Phys,](#)
896 [22, 4201–4236, <https://doi.org/10.5194/acp-22-4201-2022>, 2022.](#)

897 [Fioletov, V., McLinden, C. A., Griffin, D., Zhao, X., and Eskes, H.: Global seasonal urban, industrial, and background NO₂](#)
898 [estimated from TROPOMI satellite observations, *Atmos. Chem. Phys.*, 25, 575–596, \[https://doi.org/10.5194/acp-25-575-\]\(https://doi.org/10.5194/acp-25-575-2025\)](#)
899 [2025, 2025.](#)

900 [Fisher, B. L., Lamsal, L. N., Fasnacht, Z., Oman, L. D., Joiner, J., Krotkov, N. A., Choi, S., Qin, W., and Yang, E. S.: Revised](#)
901 [estimates of NO₂ reductions during the COVID-19 lockdowns using updated TROPOMI NO₂ retrievals and model](#)
902 [simulations, *Atmos Environ.*, 326, 120459, <https://doi.org/10.1016/J.ATMOSENV.2024.120459>, 2024.](#)

903 [Fishman, J., Iraci, L. T., Al-Saadi, J., Chance, K., Chavez, F., Chin, M., Coble, P., Davis, C., DiGiacomo, P. M., Edwards, D.,](#)
904 [Eldering, A., Goes, J., Herman, J., Hu, C., Jacob, D. J., Jordan, C., Kawa, S. R., Key, R., Liu, X., Lohrenz, S., Mannino,](#)
905 [A., Natraj, V., Neil, D., Neu, J., Newchurch, M., Pickering, K., Salisbury, J., Sosik, H., Subramaniam, A., Tzortziou, M.,](#)
906 [Wang, J., and Wang, M.: The United States’ Next Generation of Atmospheric Composition and Coastal Ecosystem](#)
907 [Measurements: NASA’s Geostationary Coastal and Air Pollution Events \(GEO-CAPE\) Mission, *Bull Am Meteorol Soc.*,](#)
908 [93, 1547–1566, <https://doi.org/10.1175/BAMS-D-11-00201.1>, 2012.](#)

909 [De Foy, B., Lu, Z., and Streets, D. G.: Satellite NO₂ retrievals suggest China has exceeded its NO_x reduction goals from the](#)
910 [twelfth Five-Year Plan, *Scientific Reports* 2016 6:1, 6, 1–9, <https://doi.org/10.1038/srep35912>, 2016.](#)

911 [Geddes, J. A., Martin, R. V., Boys, B. L., and van Donkelaar, A.: Long-term trends worldwide in ambient NO₂ concentrations](#)
912 [inferred from satellite observations, *Environ Health Perspect.*, 124, 281–289,](#)
913 [\[https://doi.org/10.1289/EHP.1409567/SUPPL_FILE/EHP.1409567.S001.ACCO.PDF\]\(https://doi.org/10.1289/EHP.1409567/SUPPL_FILE/EHP.1409567.S001.ACCO.PDF\), 2016.](#)

914 [Van Geffen, J., Eskes, H., Compernelle, S., Pinardi, G., Verhoelst, T., Lambert, J.-C., Sneep, M., Linden, M. Ter, Ludewig,](#)
915 [A., Folkert Boersma, K., and Pepijn Veeffkind, J.: Sentinel-5P TROPOMI NO₂ retrieval: impact of version v2.2](#)
916 [improvements and comparisons with OMI and ground-based data, *Atmos. Meas. Tech.*, 15, 2037–2060,](#)
917 [<https://doi.org/10.5194/amt-15-2037-2022>, 2022.](#)

918 [Ghude, S. D., Karumuri, R. K., Jena, C., Kulkarni, R., Pfister, G. G., Sajjan, V. S., Pithani, P., Debnath, S., Kumar, R., Upendra,](#)
919 [B., Kulkarni, S. H., Lal, D. M., Vander A, R. J., and Mahajan, A. S.: What is driving the diurnal variation in tropospheric](#)
920 [NO₂ columns over a cluster of high emission thermal power plants in India?, *Atmos Environ X*, 5, 100058,](#)
921 [<https://doi.org/10.1016/J.AEAOA.2019.100058>, 2020.](#)

922 [Glissenaar, I., Boersma, K. F., Anglou, I., Rijdsdijk, P., Verhoelst, T., Compernelle, S., Pinardi, G., Lambert, J.-C., Van](#)
923 [Roosendaal, M., and Eskes, H.: TROPOMI Level 3 tropospheric NO₂ dataset with advanced uncertainty analysis from](#)
924 [the ESA CCI+ ECV precursor project, *Earth Syst Sci Data*, 17, 4627–4650, <https://doi.org/10.5194/ESSD-17-4627-2025>,](#)
925 [2025.](#)

926 [Goldberg, D.: HAQAST Sentinel-5P TROPOMI Nitrogen Dioxide \(NO2\) GLOBAL Monthly Level 3 0.1 x 0.1 Degree](#)
927 [Gridded Data Version 2.4 \(HAQ_TROPOMI_NO2_GLOBAL_M_L3\) at GES DISC,](#)
928 <https://doi.org/10.5067/KKPPL39PEIGE>, 15 March 2024.

929 [Goldberg, D. L., Anenberg, S. C., Kerr, G. H., Mohegh, A., Lu, Z., and Streets, D. G.: TROPOMI NO2 in the United States:](#)
930 [A Detailed Look at the Annual Averages, Weekly Cycles, Effects of Temperature, and Correlation With Surface NO2](#)
931 [Concentrations, Earths Future, 9, https://doi.org/10.1029/2020EF001665, 2021a.](#)

932 [Goldberg, D. L., Anenberg, S. C., Lu, Z., Streets, D. G., Lamsal, L. N., E McDuffie, E., and Smith, S. J.: Urban NO x emissions](#)
933 [around the world declined faster than anticipated between 2005 and 2019, Environmental Research Letters, 16, 115004,](#)
934 <https://doi.org/10.1088/1748-9326/AC2C34>, 2021b.

935 [Goldberg, D. L., Tao, M., Kerr, G. H., Ma, S., Tong, D. Q., Fiore, A. M., Dickens, A. F., Adelman, Z. E., and Anenberg, S.](#)
936 [C.: Evaluating the spatial patterns of U.S. urban NOx emissions using TROPOMI NO2, Remote Sens Environ, 300,](#)
937 <https://doi.org/10.1016/j.rse.2023.113917>, 2024.

938 [de Gouw, J. A., Veeffkind, J. P., Roosenbrand, E., Dix, B., Lin, J. C., Landgraf, J., and Levelt, P. F.: Daily Satellite Observations](#)
939 [of Methane from Oil and Gas Production Regions in the United States, Sci Rep, 10, 1–10, https://doi.org/10.1038/S41598-](#)
940 [020-57678-4;TECHMETA=134;SUBJMETA=106,169,172,35,704,824;KWRD=ATMOSPHERIC+CHEMISTRY,](#)
941 [2020.](#)

942 [Guo, Z., Abushama, H., Siddig, K., Kirui, O. K., Abay, K., and You, L.: Monitoring Indicators of Economic Activities in](#)
943 [Sudan Amidst Ongoing Conflict Using Satellite Data, Defence and Peace Economics,](#)
944 <https://doi.org/10.1080/10242694.2023.2290474;PAGE:STRING:ARTICLE/CHAPTER>, 2023.

945 [Hajmohammadi, H. and Heydecker, B.: Evaluation of air quality effects of the London ultra-low emission zone by state-space](#)
946 [modelling, Atmos Pollut Res, 13, 101514, https://doi.org/10.1016/J.APR.2022.101514, 2022.](#)

947 [Harake, W., Jamali, I., and Abou Hamde, N.: Lebanon Economic Monitor : Lebanon Sinking \(to the Top 3\), Washington, D.C.,](#)
948 <https://doi.org/http://documents.worldbank.org/curated/en/394741622469174252>, 2021.

949 [Herman, J., Cede, A., Spinei, E., Mount, G., Tzortziou, M., and Abuhassan, N.: NO2 column amounts from ground-based](#)
950 [Pandora and MFDOAS spectrometers using the direct-sun DOAS technique: Intercomparisons and application to OMI](#)
951 [validation, Journal of Geophysical Research: Atmospheres, 114, https://doi.org/10.1029/2009JD011848, 2009.](#)

952 [Hersbach, H., Bell, B., Berrisford, P., Hirahara, S., Horányi, A., Muñoz-Sabater, J., Nicolas, J., Peubey, C., Radu, R., Schepers,](#)
953 [D., Simmons, A., Soci, C., Abdalla, S., Abellan, X., Balsamo, G., Bechtold, P., Biavati, G., Bidlot, J., Bonavita, M., De](#)
954 [Chiara, G., Dahlgren, P., Dee, D., Diamantakis, M., Dragani, R., Flemming, J., Forbes, R., Fuentes, M., Geer, A.,](#)
955 [Haimberger, L., Healy, S., Hogan, R. J., Hólm, E., Janisková, M., Keeley, S., Laloyaux, P., Lopez, P., Lupu, C., Radnoti,](#)

956 [G., de Rosnay, P., Rozum, I., Vamborg, F., Villaume, S., and Thépaut, J. N.: The ERA5 global reanalysis, Quarterly](#)
957 [Journal of the Royal Meteorological Society, 146, 1999–2049, <https://doi.org/10.1002/QJ.3803>, 2020.](#)

958 [Hilboll, A., Richter, A., and Burrows, J. P.: Sciences ess Atmospheric Chemistry and Physics Climate of the Past Geoscientific](#)
959 [Instrumentation Methods and Data Systems Long-term changes of tropospheric NO 2 over megacities derived from](#)
960 [multiple satellite instruments, Atmos. Chem. Phys. 13, 4145–4169, <https://doi.org/10.5194/acp-13-4145-2013>, 2013.](#)

961 [Ho, C. H., Heo, J. W., Chang, M., Choi, W., Kim, J., Kim, S. W., and Oh, H. R.: Regulatory measures significantly reduced](#)
962 [air-pollutant concentrations in Seoul, Korea, Atmos Pollut Res, 12, 101098, <https://doi.org/10.1016/J.APR.2021.101098>,](#)
963 [2021.](#)

964 [Hoesly, R. M., Smith, S. J., Ahsan, H., Prime, N., O'Rourke, P., Crippa, M., Klimont, Z., Guizzardi, D., Feng, L., Harkins, C.,](#)
965 [McDonald, B. C., & Wang, S: CEDS v 2025_04_18 Gridded Data 0.1 degree. Zenodo.](#)
966 <https://doi.org/10.5281/zenodo.15001545>, 2025.

967 [Huber, D. E., Kort, E. A., and Steiner, A. L.: Soil Moisture, Soil NOx and Regional Air Quality in the Agricultural Central](#)
968 [United States, Journal of Geophysical Research: Atmospheres, 129, e2024JD041015,](#)
969 <https://doi.org/10.1029/2024JD041015>, 2024.

970 [Jiang, Z., McDonald, B. C., Worden, H., Worden, J. R., Miyazaki, K., Qu, Z., Henze, D. K., Jones, D. B. A., Arellano, A. F.,](#)
971 [Fischer, E. V., Zhu, L., and Folkert Boersma, K.: Unexpected slowdown of US pollutant emission reduction in the past](#)
972 [decade, Proc Natl Acad Sci U S A, 115, 5099–5104, <https://doi.org/10.1073/PNAS.1801191115/-/DCSUPPLEMENTAL>,](#)
973 [2018.](#)

974 [Jiang, Z., Zhu, R., Miyazaki, K., McDonald, B. C., Klimont, Z., Zheng, B., Boersma, K. F., Zhang, Q., Worden, H., Worden,](#)
975 [J. R., Henze, D. K., Jones, D. B. A., Denier van der Gon, H. A. C., and Eskes, H.: Decadal Variabilities in Tropospheric](#)
976 [Nitrogen Oxides Over United States, Europe, and China, Journal of Geophysical Research: Atmospheres, 127,](#)
977 [e2021JD035872, <https://doi.org/10.1029/2021JD035872>, 2022.](https://doi.org/10.1029/2021JD035872)

978 [Jin, X., Zhu, Q., Cohen, R. C., and Xiaomeng, J.: Direct estimates of biomass burning NO x emissions and lifetimes using](#)
979 [daily observations from TROPOMI, Atmos. Chem. Phys, 21, 15569–15587, <https://doi.org/10.5194/acp-21-15569-2021>,](#)
980 [2021.](#)

981 [Kim, E. J., Holloway, T., Kokandakar, A., Harkey, M., Elkins, S., Goldberg, D. L., and Heck, C.: A Comparison of Regression](#)
982 [Methods for Inferring Near-Surface NO2 With Satellite Data, Journal of Geophysical Research: Atmospheres, 129,](#)
983 [e2024JD040906, <https://doi.org/10.1029/2024JD040906>, 2024.](https://doi.org/10.1029/2024JD040906)

984 [Krotkov, N. A., Mclinden, C. A., Li, C., Lamsal, L. N., Celarier, E. A., Marchenko, S. V, Swartz, W. H., Bucsele, E. J., Joiner,](#)
985 [J., Duncan, B. N., Folkert Boersma, K., Pepijn Veefkind, J., Levelt, P. F., Fioletov, V. E., Dickerson, R. R., He, H., Lu,](#)

986 [Z., and Streets, D. G.: Aura OMI observations of regional SO₂ and NO₂ pollution changes from 2005 to 2015, Atmos.](#)
987 [Chem. Phys, 16, 4605–4629, <https://doi.org/10.5194/acp-16-4605-2016>, 2016.](#)

988 [Labzovskii, L. D., Belikov, D. A., and Damiani, A.: Spaceborne NO₂ observations are sensitive to coal mining and processing](#)
989 [in the largest coal basin of Russia, Sci Rep, 12, 1–11, \[https://doi.org/10.1038/S41598-022-16850-\]\(https://doi.org/10.1038/S41598-022-16850-8\)](#)
990 [8;SUBJMETA=106,172,35,4081,704;KWRD=ATMOSPHERIC+SCIENCE,ENVIRONMENTAL+IMPACT,ENVIRO](#)
991 [NMENTAL+SCIENCES, 2022.](#)

992 [Lambert, J.-C.: Quarterly Validation Report of the Copernicus Sentinel-5 Precursor Operational Data Products #28: April 2018](#)
993 [– August 2025, 227 pp., 2025.](#)

994 [Lamsal, L. N., Duncan, B. N., Yoshida, Y., Krotkov, N. A., Pickering, K. E., Streets, D. G., and Lu, Z.: U.S. NO₂ trends](#)
995 [\(2005–2013\): EPA Air Quality System \(AQS\) data versus improved observations from the Ozone Monitoring Instrument](#)
996 [\(OMI\), Atmos Environ, 110, 130–143, <https://doi.org/10.1016/J.ATMOSENV.2015.03.055>, 2015.](#)

997 [Laughner, J. L. and Cohen, R. C.: Direct observation of changing NO_x lifetime in North American cities, Science \(1979\), 366,](#)
998 [723–727, <https://doi.org/https://doi.org/10.1126/science.aax6832>, 2019.](#)

999 [Levelt, P. F., Van Den Oord, G. H. J., Dobber, M. R., Mälkki, A., Visser, H., De Vries, J., Stammes, P., Lundell, J. O. V., and](#)
1000 [Saari, H.: The ozone monitoring instrument, IEEE Transactions on Geoscience and Remote Sensing, 44, 1093–1100,](#)
1001 [https://doi.org/10.1109/TGRS.2006.872333, 2006.](#)

1002 [Levelt, P. F., Stein Zweers, D. C., Aben, I., Bauwens, M., Borsdorff, T., De Smedt, I., Eskes, H. J., Lerot, C., Loyola, D. G.,](#)
1003 [Romahn, F., Stavrou, T., Theys, N., Van Roozendaal, M., Veeffkind, J. P., and Verhoelst, T.: Air quality impacts of](#)
1004 [COVID-19 lockdown measures detected from space using high spatial resolution observations of multiple trace gases](#)
1005 [from Sentinel-5P/TROPOMI, Atmos Chem Phys, 22, 10319–10351, <https://doi.org/10.5194/ACP-22-10319-2022>, 2022.](#)

1006 [Li, H., Zheng, B., Lei, Y., Hauglustaine, D., Chen, C., Lin, X., Zhang, Y., Zhang, Q., and He, K.: Trends and drivers of](#)
1007 [anthropogenic NO_x emissions in China since 2020, Environmental Science and Ecotechnology, 21, 100425,](#)
1008 [https://doi.org/10.1016/J.ESE.2024.100425, 2024.](#)

1009 [Liu, B., Fu, X., Bechtel, A., Gross, D., Sachsenhofer, R. F., and Li, X.: Middle Permian environmental changes and shale oil](#)
1010 [potential evidenced by high-resolution organic petrology, geochemistry and mineral composition of the sediments in the](#)
1011 [Santanghu Basin, Northwest China, Int J Coal Geol, 185, 119–137, <https://doi.org/10.1016/J.COAL.2017.11.015>, 2018.](#)

1012 [Liu, F., Zhang, Q., Van Der A, R. J., Zheng, B., Tong, D., Yan, L., Zheng, Y., and He, K.: Recent reduction in NO_x emissions](#)
1013 [over China: synthesis of satellite observations and emission inventories, Environmental Research Letters, 11, 114002,](#)
1014 [https://doi.org/10.1088/1748-9326/11/11/114002, 2016.](#)

1015 [Lonsdale, C. R. and Sun, K.: Nitrogen oxides emissions from selected cities in North America, Europe, and East Asia observed](#)
1016 [by the TROPOspheric Monitoring Instrument \(TROPOMI\) before and after the COVID-19 pandemic, Atmos. Chem.](#)
1017 [Phys, 23, 8727–8748, <https://doi.org/10.5194/acp-23-8727-2023>, 2023.](#)

1018 [Ma, Q., Wang, J., Xiong, M., and Zhu, L.: Air Quality Index \(AQI\) Did Not Improve during the COVID-19 Lockdown in](#)
1019 [Shanghai, China, in 2022, Based on Ground and TROPOMI Observations, Remote Sens \(Basel\), 15, 1295,](#)
1020 <https://doi.org/10.3390/RS15051295/S1>, 2023.

1021 [Martínez-Alonso, S., Veeffkind, J. P., Dix, B., Gaubert, B., Theys, N., Granier, C., Soulié, A., Darras, S., Eskes, H., Tang, W.,](#)
1022 [Worden, H., de Gouw, J., and Levelt, P. F.: S-5P/TROPOMI-Derived NO_x Emissions From Copper/Cobalt Mining and](#)
1023 [Other Industrial Activities in the Copperbelt \(Democratic Republic of Congo and Zambia\), Geophys Res Lett, 50,](#)
1024 [e2023GL104109, <https://doi.org/10.1029/2023GL104109>, 2023.](https://doi.org/10.1029/2023GL104109)

1025 [Matthias, V., Quante, M., Arndt, J. A., Badeke, R., Fink, L., Petrik, R., Feldner, J., Schwarzkopf, D., Link, E. M., Ramacher,](#)
1026 [M. O. P., and Wedemann, R.: The role of emission reductions and the meteorological situation for air quality](#)
1027 [improvements during the COVID-19 lockdown period in central Europe, Atmos Chem Phys, 21, 13931–13971,](#)
1028 <https://doi.org/10.5194/ACP-21-13931-2021>, 2021.

1029 [Miyazaki, K., Eskes, H., Sudo, K., Folkert Boersma, K., Bowman, K., and Kanaya, Y.: Decadal changes in global surface NO_x](#)
1030 [emissions from multi-constituent satellite data assimilation, Atmos Chem Phys, 17, 807–837,](#)
1031 <https://doi.org/10.5194/ACP-17-807-2017>, 2017.

1032 [Panda, M. R., Tyagi, A., Dhanya, C. T., Verma, A., and Swain, A.: Vulnerability assessment of thermal power plants in India](#)
1033 [under water stress conditions, Energy, 276, 127553, <https://doi.org/10.1016/J.ENERGY.2023.127553>, 2023.](#)

1034 [Richter, A., Burrows, J. P., Nüß, H., Granier, C., and Niemeier, U.: Increase in tropospheric nitrogen dioxide over China](#)
1035 [observed from space, Nature, 437, 129–132, <https://doi.org/10.1038/nature04092>, 2005.](#)

1036 [Rokicki, T., Bórawski, P., and Szeberényi, A.: The Impact of the 2020–2022 Crises on EU Countries’ Independence from](#)
1037 [Energy Imports, Particularly from Russia, Energies 2023, Vol. 16, Page 6629, 16, 6629,](#)
1038 <https://doi.org/10.3390/EN16186629>, 2023.

1039 [Schiavina M., Melchiorri M. & Pesaresi M.: GHS-SMOD R2023A - GHS settlement layers, application of the Degree of](#)
1040 [Urbanisation methodology \(stage I\) to GHS-POP R2023A and GHS-BUILT-S R2023A, multitemporal \(1975-2030\).](#)
1041 [European Commission, Joint Research Centre \(JRC\). \[https://doi.org/10.2905/A0DF7A6F-49DE-46EA-9BDE-\]\(https://doi.org/10.2905/A0DF7A6F-49DE-46EA-9BDE-563437A6E2BA\)](#)
1042 [563437A6E2BA](https://doi.org/10.2905/A0DF7A6F-49DE-46EA-9BDE-563437A6E2BA), 2023.

1043 [Schumann, U. and Huntrieser, H.: The global lightning-induced nitrogen oxides source, Atmos. Chem. Phys, 7, 3823–3907,](#)
1044 [2007.](https://doi.org/10.5194/acp-7-3823-2007)

1045 [Seo, S., Kim, S. W., Kim, K. M., Lamsal, L. N., and Jin, H.: Reductions in NO₂ concentrations in Seoul, South Korea detected](#)
1046 [from space and ground-based monitors prior to and during the COVID-19 pandemic, Environ Res Commun, 3, 051005,](#)
1047 <https://doi.org/10.1088/2515-7620/ABED92>, 2021.

1048 [Shi, Q., Zheng, B., Zheng, Y., Tong, D., Liu, Y., Ma, H., Hong, C., Geng, G., Guan, D., He, K., and Zhang, Q.: Co-benefits of](#)
1049 [CO₂ emission reduction from China's clean air actions between 2013-2020, Nature Communications 2022 13:1, 13, 1–8,](#)
1050 <https://doi.org/10.1038/s41467-022-32656-8>, 2022.

1051 [Shikwambana, L., Mhangara, P., and Mbatha, N.: Trend analysis and first time observations of sulphur dioxide and nitrogen](#)
1052 [dioxide in South Africa using TROPOMI/Sentinel-5 P data, International Journal of Applied Earth Observation and](#)
1053 [Geoinformation, 91, 102130, https://doi.org/10.1016/J.JAG.2020.102130](#), 2020.

1054 [Song, W., Liu, X. Y., Hu, C. C., Chen, G. Y., Liu, X. J., Walters, W. W., Michalski, G., and Liu, C. Q.: Important contributions](#)
1055 [of non-fossil fuel nitrogen oxides emissions, Nature Communications 2021 12:1, 12, 1–7, https://doi.org/10.1038/s41467-](#)
1056 [020-20356-0](#), 2021.

1057 [Stavrakou, T., Müller, J.-F., Boersma, K. F., De Smedt, I., and van der A, R. J.: Assessing the distribution and growth rates of](#)
1058 [NO_x emission sources by inverting a 10-year record of NO₂ satellite columns, Geophys Res Lett, 35,](#)
1059 <https://doi.org/10.1029/2008GL033521>, 2008.

1060 [VanDerA, R. J., Eskes, H. J., Boersma, K. F., van Noije, T. P. C., Van Roozendaal, M., De Smedt, I., Peters, D. H. M. U., and](#)
1061 [Meijer, E. W.: Trends, seasonal variability and dominant NO_x source derived from a ten year record of NO₂ measured](#)
1062 [from space, Journal of Geophysical Research Atmospheres, 113, 1–12, https://doi.org/10.1029/2007JD009021](#), 2008.

1063 [Varma, A. K., Biswal, S., Hazra, B., Mendhe, V. A., Misra, S., Samad, S. K., Singh, B. D., Dayal, A. M., and Mani, D.:](#)
1064 [Petrographic characteristics and methane sorption dynamics of coal and shaly-coal samples from Ib Valley Basin, Odisha,](#)
1065 [India, Int J Coal Geol, 141–142, 51–62, https://doi.org/10.1016/J.COAL.2015.03.005](#), 2015.

1066 [Veefkind, J. P., Aben, I., McMullan, K., Förster, H., de Vries, J., Otter, G., Claas, J., Eskes, H. J., de Haan, J. F., Kleipool, Q.,](#)
1067 [van Weele, M., Hasekamp, O., Hoogeveen, R., Landgraf, J., Snel, R., Tol, P., Ingmann, P., Voors, R., Kruizinga, B., Vink,](#)
1068 [R., Visser, H., and Levelt, P. F.: TROPOMI on the ESA Sentinel-5 Precursor: A GMES mission for global observations](#)
1069 [of the atmospheric composition for climate, air quality and ozone layer applications, Remote Sens Environ, 120, 70–83,](#)
1070 <https://doi.org/10.1016/J.RSE.2011.09.027>, 2012.

1071 [Vlemmix, T., Piders, A. J. M., Stammes, P., Wang, P., and Levelt, P. F.: Retrieval of tropospheric NO₂ using the MAX-DOAS](#)
1072 [method combined with relative intensity measurements for aerosol correction, Atmos Meas Tech, 3, 1287–1305,](#)
1073 <https://doi.org/10.5194/AMT-3-1287-2010>, 2010.

1074 [Wang, C., Wang, T., and Wang, P.: The Spatial–Temporal Variation of Tropospheric NO₂ over China during 2005 to 2018,](#)
1075 [Atmosphere 2019, Vol. 10, Page 444, 10, 444, https://doi.org/10.3390/ATMOS10080444](#), 2019.

- 1076 [Zhang, Y., Tian, J., Feng, S., Yang, F., and Lu, X.: The occurrence modes and geologic origins of arsenic in coal from](#)
1077 [Santanghu Coalfield, Xinjiang, J Geochem Explor, 186, 225–234, <https://doi.org/10.1016/J.GEXPLO.2017.12.006>, 2018.](#)
- 1078 [Zhao, X., Li, X. X., Xin, R., Zhang, Y., and Liu, C. H.: Impact of Lockdowns on Air Pollution: Case Studies of Two Periods](#)
1079 [in 2022 in Guangzhou, China, Atmosphere 2024, Vol. 15, Page 1144, 15, 1144,](#)
1080 [<https://doi.org/10.3390/ATMOS15091144>, 2024.](#)
- 1081 [Zheng, B., Zhang, Q., Geng, G., Chen, C., Shi, Q., Cui, M., Lei, Y., and He, K.: Changes in China's anthropogenic emissions](#)
1082 [and air quality during the COVID-19 pandemic in 2020, Earth Syst Sci Data, 13, 2895–2907,](#)
1083 [<https://doi.org/10.5194/ESSD-13-2895-2021>, 2021.](#)